scientific reports

Check for updates

OPEN

Design, synthesis, biological evaluation, and in silico characterization of chalcone derivatives as antidiabetic hits

Arif Ali[1,8], Frederico de Bastos Oliveira Dias[2,8], Gabriela Ramos Borges[3], Zubair Hussain[4], Amir Zada[1], Gustavo S. S. Felizardo[5], Tiago Elias Allievi Frizon[6], Fethi Ahmet Ozdemir[7], Ahmet Çetin[7], Mohammad Naeem[1], Luiz Henrique Keng Queiroz Júnior[2], Bruno Junior Neves[5], Muhammad Ishaq Ali Shah[1]✉, Jamal Rafique[2,3]✉ & Sumbal Saba[2]✉

A series of 40 chalcone derivatives was synthesized through Claisen–Schmidt condensation and characterized by FT-IR and NMR spectroscopy. The compounds were evaluated for α-amylase inhibitory and DPPH radical-scavenging activities to identify chalcone-based hits with a dual in vitro profile relevant to postprandial glycemic control. The series displayed a broad range of activities, with α-amylase IC_{50}, values spanning 10.41 ± 1.23–1021.64 ± 2.75 µM and radical-scavenging IC_{50}, values ranging from 31.34 ± 0.20 to 698.34 ± 14.56 µM. Among the evaluated compounds, 4, 17, 19, 31, 33, and 35 emerged as the most active α-amylase inhibitors, with compound 4 being the most potent member of the series (IC_{50} = 10.41 ± 1.23 µM), outperforming acarbose (IC_{50} = 73.12 ± 5.04 µM). Structure–activity relationship analysis indicated that hydroxy- and methoxy-substituted aryl motifs were generally favorable, whereas some heteroaryl replacements and heavily halogenated patterns were less well tolerated. To rationalize the experimental profile, an ensemble docking workflow coupled to Naive Bayes rescoring was applied to human pancreatic α-amylase. The predicted binding modes supported productive occupation of the catalytic groove and suggested a key interaction between compound 4 and Glu233, consistent with its superior inhibitory potency. In silico ADMET profiling of the leading compounds indicated acceptable lipophilicity, solubility, intestinal absorption, and low predicted cardiotoxicity, with compound 4 showing the most balanced overall profile. In summary, these findings identify this chalcone series as a promising starting point for hit-to-lead optimization toward multifunctional radical scavenging and α-amylase inhibitors.

Keywords Chalcones, α-Amylase inhibitors, Free radical scavengers, Structure–activity relationship, Molecular docking

Diabetes mellitus remains a major global health burden characterized by chronic hyperglycemia, resulting from impaired insulin secretion, insulin resistance in target tissues, or a combination of these defects. Beyond glycemic dysregulation, sustained hyperglycemia promotes progressive damage to the vasculature, kidney, retina, and heart, thereby contributing to substantial morbidity, mortality, and healthcare expenditure[1–3]. Accordingly, identifying small molecules capable of controlling postprandial glucose excursions while exhibiting suitable pharmacological properties remains an important objective in antidiabetic drug discovery[4–6].

[1]Department of Chemistry, Abdul Wali Khan University, Mardan 23200, Khyber Pakhtunkhwa, Pakistan. [2]Laboratory of Sustainable Synthesis and Organochalcogen (LabSO), Instituto de Química (IQ), Universidade Federal de Goiás – UFG, Goiânia, GO 74690-900, Brazil. [3]Instituto de Química (INQUI), Universidade Federal Do Mato Grosso Do Sul - UFMS, Campo Grande, MS 79074-460, Brazil. [4]National Institute for Biotechnology and Genetic Engineering College, Pakistan Institute of Engineering and Applied Sciences, Faisalabad 44000, Pakistan. [5]Laboratory of Cheminformatics (LCi), Faculdade de Farmácia, Universidade Federal de Goiás – UFG, 74605-170, Goiânia, GO, Brazil. [6]Department of Chemistry, Universidade Federal de Santa Catarina, Florianópolis, Santa Catarina 88040-900, Brazil. [7]Faculty of Science and Art, Bingöl University, Bingöl 1200, Türkiye. [8]Arif Ali and Frederico de Bastos Oliveira Dias both authors contributed equally to this work. ✉email: ishaqalishah@awkum.edu.pk; jamal.rafique@ufms.br; jamal.chm@gmail.com; sumbalsaba@ufg.br

Among the validated strategies for postprandial glycemic control, inhibition of digestive enzymes involved in carbohydrate processing is particularly attractive[7–9]. In this context, α-Amylase (EC 3.2.1.1) catalyzes the initial hydrolysis of dietary polysaccharides by cleaving α-1,4-glycosidic bonds, producing smaller oligosaccharides that are subsequently converted into absorbable glucose by α-glucosidase. Pharmacological inhibition of α-amylase can therefore attenuate intestinal glucose release and reduce postprandial hyperglycemia[10–12]. However, clinically available carbohydrate-hydrolyzing enzyme inhibitors such as acarbose, miglitol, and voglibose are commonly associated with gastrointestinal adverse effects, highlighting the need for new chemotypes with improved potency and a more balanced overall profile[13,14].

In parallel, poorly controlled hyperglycemia and the associated complications of DM dysregulate oxidoreductase enzymes, including xanthine oxidase and lipoxygenase, thereby increasing the generation of reactive oxygen species (ROS), reactive nitrogen species (RNS), and other free radicals during metabolism[15]. These highly reactive species can damage biomacromolecules such as proteins, lipids, and DNA, triggering oxidative chain reactions that contribute to cellular dysfunction and tissue injury[16–20]. Sustained oxidative and nitrosative stress can ultimately promote cell death and progressive tissue injury, contributing to pathological alterations in vital organs, including the heart, kidneys, liver, and immune system, and thereby favoring the development of inflammatory, cardiovascular, neoplastic, arthritic, and age-related disorders[21–26]. In this context, diabetic complications can be managed through controlling ROS and RNS[27–29]. From a medicinal chemistry standpoint, this provides a compelling rationale for exploring multifunctional molecules able to combine α-amylase inhibition with radical-scavenging capacity within a single scaffold[30–32].

Chalcones (1,3-diphenylprop-2-en-1-ones) constitute a privileged and synthetically tractable chemotype for this purpose[33–35]. Their α,β-unsaturated ketone framework, which links two aromatic or heteroaromatic fragments, enables broad structural diversification (Fig. 1). They provide a safe and straightforward synthetic platform for accessing a wide range of biologically relevant heterocycles, including dihydropyrazole[36], azachalcone[37], pyrimidine[38], cyanopyridine, pyrazoline[39], isoxazole, while also being structurally related to natural isoflavonoids, flavonoids, and aurones, which has placed them at the center of considerable medicinal chemistry interest[40]. Moreover, their scaffold readily accommodates hydroxy-, methoxy-, halo-, and heteroaryl substituents, allowing precise modulation of electronic distribution, hydrogen-bonding capacity, and lipophilic balance. This sustained interest is also consistent with the wide range of biological activities reported for chalcone derivatives across different therapeutic contexts[41–59]. This translational relevance is further supported by clinically used or investigated chalcone-based agents (Fig. 1), such as metochalcone (**i**)[60] and sofalcone (**ii**)[61], as well as hesperidin methylchalcone (**iii**) and trimethylchalcone (**iv**)[62], which have shown therapeutic utility in gastrointestinal and venous disorders.

Currently, different chalcone scaffold such as metochalcone(**i**)[60], and sofalcone(**ii**)[61], have been investigated in clinical practice and are approved as choleretic and antiulcer drug as shown in Fig. 1. Likewise, hespiridine methylchalcone(**iii**), and trimethylchalcone(**iv**), clinical investigations in chronic venous lymphatic insufficiency, trunk and branch varicosis show it more effective in relieving of symptoms and show excellent tolerance level[62].

The above interesting biological potentials of the chalcone scaffold in drug discovery, and the associated challenges to already in use drugs against DM, have made the situation more interesting and highly pressing to develop more novel and efficient drugs. Here in this work our focus is to use chalcone analogues as the main scaffold in the integral project to develop novel agent having *α*-amylase inhibition and free radical scavenging features. As part of our research interest in synthesis of biologically relevant compounds[63–77] and keeping in mind the above-mentioned objectives, we have synthesized various analogues of chalcone by using different types of substituted aldehyde and acetophenone, after purification and structural characterization their α-amylase inhibition and free radical scavenging potential were evaluated. Further, the molecular docking, and ADMET studies were conducted.

Materials and methods

Experimental methods

Synthesis and characterization of compounds

All chemicals and reagents were synthetic grade, obtained from commercial sources, and used without further purification unless stated otherwise. Specifically, aromatic aldehydes, acetophenones, sodium hydroxide, and

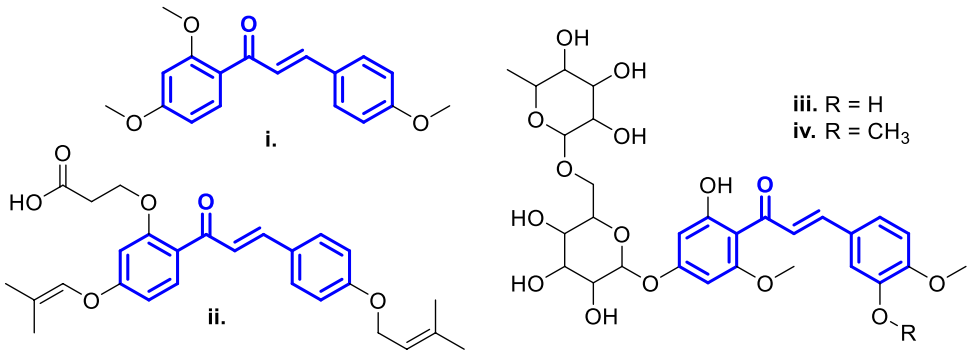

Fig. 1. Representative chalcones, clinically investigated and approved.

common solvents were purchased from Alfa Aesar. Reaction progress was tracked by thin-layer chromatography (TLC) on Merck silica gel plates. Purification of final products was achieved by recrystallization from absolute ethanol. Infrared spectra were acquired on a Shimadzu Fourier-transform infrared (FT-IR) spectrometer. Nuclear magnetic resonance (NMR) spectra (^{1}H and ^{13}C) were recorded in deuterated DMSO or $CDCl_3$ using Bruker 400/600 MHz and 100/125 MHz spectrometers, respectively.

General protocol for the synthesis of compounds

For the synthesis of various chalcone derivatives, the Claisen–Schmidt reaction described in the literature was used with minimal modification[78]. An aqueous solution of NaOH (3 M, 3 mL) was added to a solution of aromatic ketone (3 mmol) in EtOH. The resulting solution was stirred at room temperature for a while, then an ethanolic solution of various substituted aldehydes was added dropwise to the reaction mixture. After complete addition of aldehydes, the reaction mixture was stirred at room temperature for 24 h; the reaction progress was monitored by thin-layer chromatography (TLC) at regular intervals. After the reaction was completed, the mixture was cooled and left to stand for 24 h. Then, the residue was collected, and the product was separated, washed with water, and then air-dried. The target compounds were purified by recrystallization from absolute EtOH. The resultant compounds (**1–40**) were characterized by various spectroscopic techniques. The spectroscopic data for the synthesized compounds are presented below, and their spectra are shown in the supporting information (Figures SS1-SS80).

Spectral data of synthesized compounds

(E)-1-(4-chlorophenyl)-3-(4-methoxyphenyl)prop-2-en-1-one (1): Yield: 78%; white crystalline solid; MP: 118–120 °C (lit. = 120–121 °C)[79]; Rf. value: 0.4 (Ethyl acetate/n-hexane,1:4); FT-IR (KBr, cm^{-1}): 3027, 1680, 1590,1550,1505,1250,1020. ^{1}H-NMR(600 MHz, $CDCl_3$): 7.97(2H, d, *J* = 8.40), 7.81(1H, d, *J* = 15.60), 7.61(2H, d, *J* = 8.50), 7.47(2H, d, *J* = 8.40), 7.38(1H, d, *J* = 15.60), 6.95(2H, d, *J* = 8.50), 3.86(3H, s, -OCH_3). ^{13}C-NMR (150 MHz, $CDCl_3$): 189.00, 162.12, 145.39, 139.27, 136.61, 130.31, 129.82, 128.85, 127.47, 119.20, 114.45, 55.41.

(E)-1-(4-chlorophenyl)-3-(p-tolyl)prop-2-en-1-one (2): Yield: 78%; white crystalline solid; MP: 165 °C (lit. = 163–164 °C)[80]; Rf. value: 0.4 (Ethyl acetate/n-hexane,1:4); FT-IR (KBr, cm^{-1}): 3065,1665,1605,1545,1515,1260,1020. ^{1}H-NMR(400 MHz, $CDCl_3$): 8.08(2H, d, *J* = 8.60), 7.93(1H, d, *J* = 15.60), 7.66(2H, d, *J* = 8.00), 7.59(2H, d, *J* = 8.60), 7.57(1H, d, *J* = 15.60), 6.35(2H, d, *J* = 8.00), 2.50(3H, s, -CH_3). ^{13}C-NMR(100 MHz, $CDCl_3$): 189.38, 145.45, 141.33, 139.07, 136.65, 131.97, 129.88, 129.76, 128.90, 128.56, 120.47, 21.53.

(E)-1-(4-chlorophenyl)-3-phenylprop-2-en-1-one (3): Yield**:** 80%; off white crystalline solid; MP: 116–118 °C (lit. = 113–117 °C)[81]; Rf. value: 0.40 (Ethyl acetate/n-hexane,1:4); FT-IR (KBr, cm $^{-1}$): 3018, 1655, 1600, 1575, 1520, 1260, 1015. ^{1}H-NMR(400 MHz, $CDCl_3$): 8.05(2H, d, *J* = 8.30), 7.91(1H, d, *J* = 15.60), 7.72–7.69(2H, m), 7.59(1H, d, *J* = 15.60), 7.54(2H, d, *J* = 8.60), 7.50–7.48(3H, m). ^{13}C-NMR(100 MHz, $CDCl_3$): 189.03, 145.18, 136.35, 134.57, 130.86, 129.93, 129.00, 128.92, 128.55, 121.39.

(E)-1-(4-chlorophenyl)-3-(2-hydroxyphenyl)prop-2-en-1-one (4): Yield: 72%; red color solid; MP: 113–115 °C (lit. = 115–120 °C)[82]; Rf. value: 0.35 (Ethyl acetate/n-hexane,1:4); FT-IR (KBr, cm $^{-1}$): 3450,3013, 1655, 1590, 1570, 1510, 1235, 1005. ^{1}H-NMR(600 MHz, DMSO-d_6): 10.29 (s, 1H, -OH), 8.13(2H, d, *J* = 8.60), 8.08(1H, d, *J* = 15.70), 7.87(1H, d, *J* = 7.80), 7.85(1H, d, *J* = 15.70), 7.64(2H, d, *J* = 8.60), 7.30(1H, t, *J* = 5.76), 6.96(1H, d, *J* = 8.16), 6.90(1H, t, *J* = 7.68). ^{13}C-NMR (150 MHz, DMSO-d_6): 188.23, 157.18, 139.91, 137.79, 136.57, 132.12, 128.83, 128.73, 121.29, 120.60, 119.39, 116.25.

(E)-1-(4-chlorophenyl)-3-(furan-2-yl)prop-2-en-1-one (5): Yield: 85%; cream/yellow color solid; MP: 75–76 °C (lit. = 72–74 °C)[83]; Rf.value:0.5 (Ethyl acetate/n-hexane,1:4); FT-IR(KBr, cm^{-1}): 3100, 1655, 1595, 1510, 1315. ^{1}H-NMR(400 MHz, DMSO-d_6): 8.16(2H, d, *J* = 8.50), 8.0(1H, d, J = 3.30), 7.69(2H, d, *J* = 8.50), 7.65(1H, d, *J* = 15.40), 7.56(1H, d, *J* = 15.40), 7.21(1H, d, *J* = 3.40), 6.78–7.77(1H, m). ^{13}C-NMR(100 MHz, DMSO-d_6): 188.0, 151.51, 146.80, 138.45, 136.39, 131.30, 130.61, 129.35, 118.78, 117.84, 113.64.

(E)-1-(4-chlorophenyl)-3-(3-nitrophenyl)prop-2-en-1-one (6): Yield: 80%; off white amorphous solid; MP: 116–118 °C (lit. = 119 °C)[84]; Rf. value: 0.4 (Ethyl acetate/n-hexane,1:4); FT-IR (KBr, cm^{-1}): 3095, 1662, 1602, 1510, 1325. ^{1}H-NMR(400 MHz, $CDCl_3$): 8.53 (1H, s), 8.29(1H, d, *J* = 7.70), 8.08(2H, d, *J* = 9.90), 7.76(1H, d, *J* = 7.70), 7.87(1H, d, *J* = 15.70), 7.70(1H, d, *J* = 15.70), 7.65(2H, d, *J* = 9.90), 7.58(1H, t, *J* = 7.80). ^{13}C-NMR (100 MHz, DMSO- d_6): 189.47, 148.94, 141.63, 137.77, 137.09, 135.32, 133.74, 130.74, 129.21, 129.10, 125.47, 124.98, 123.47.

(E)-1-(4-chlorophenyl)-3-(4-(dimethylamino)phenyl)prop-2-en-1-one (7): Yield: 82%; deep yellow crystalline solid.; MP: 134–136 °C (lit. = 138–140 °C)[79]; Rf. Value: 0.5 (Ethyl acetate/n-hexane,1:4); FT-IR (KBr, cm^{-1}): 3040, 1645, 1590, 1560, 1510, 1255, 1015. ^{1}H-NMR(600 MHz, DMSO-d_6): 8.13(2H, d, *J* = 8.50), 7.72(2H, d, *J* = 8.40), 7.69(1H, d, *J* = 16.0), 7.63(1H, d, *J* = 16.0), 7.60(2H, d, *J* = 8.40), 6.76 (2H, d, *J* = 8.50), 3.01(6H, s, -$N(CH_3)_2$). ^{13}C-NMR (150 MHz, DMSO-d_6): 187.51, 152.20, 145.75, 137.41, 136.98, 130.82, 130.02, 128.76, 121.93, 115.75, 111.64, 39.65.

(E)-1-(4-chlorophenyl)-3-(3H-pyrrol-2-yl)prop-2-en-1-one (8): Yield: 72%; deep yellow crystalline solid; MP: 173–175 °C (lit. = 175 °C)[85,86]; Rf. Value: 0.50 (Ethyl acetate/n-hexane,1:4); FT-IR (KBr, cm $^{-1}$): 3055, 1635 ,1570, 1545, 1520, 1235, 1025. ^{1}H-NMR(400 MHz, DMSO-d_6): 11.83 (1H, s, -NH), 8.14(2H, d, *J* = 8.60), 7.74(1H, d, *J* = 15.50), 7.71(2H, d, *J* = 8.60), 7.66(1H, d, *J* = 15.50), 7.26–7.24(1H, m), 6.86–6.84(1H, m), 6.34–6.32(1H, m). ^{13}C-NMR(100 MHz, DMSO-d_6): 189.47, 148.94, 141.63, 137.77, 137.09, 135.32, 133.74, 130.74, 129.21, 129.10, 125.47, 124.98, 123.47.

(E)-1-(4-chlorophenyl)-3-(3,4,5-trimethoxyphenyl)prop-2-en-1-one (9): Yield: 73%; light yellow crystalline solid; MP: 105–107 °C (lit. = 105 °C)[87,88]; Rf. value:0.43 (Ethylacetate/n-hexane,1:4); FT-IR (KBr, cm^{-1}):3065,1635,1580,1565,1510,1235,1020. ^{1}H-NMR(400 MHz, $CDCl_3$): 8.07(2H, d, *J* = 8.60), 7.84(1H, d, *J* = 15.60), 7.59(2H, d, *J* = 8.60), 7.48(1H, d, *J* = 15.60), 6.96(1H, s), 4.02(6H, s, -2OCH_3), 4.01(3H, s, -OCH_3).

^{13}C-NMR (100 MHz, $CDCl_3$): 189.22, 153.55, 145.69, 139.15, 136.74, 130.11, 129.92, 128.95, 120.84, 105.76, 61.01, 56.37.

(E)-1-(4-chlorophenyl)-3-(thiophen-2-yl)prop-2-en-1-one (10): Yield: 74% ; light yellow crystalline solid; MP: 119–121 °C (lit. = 118–120 °C)[83]; Rf. value: 0.38 (EtOAc/n-hexane,1:4); FT- IR (KBr, cm $^{-1}$): 3057, 1630, 1560, 1525, 1490, 1225, 1005 ^{1}H-NMR(400 MHz, $CDCl_3$): 8.09(1H, d, *J* = 15.20), 8.05(2H, d, *J* = 8.70), 7.60(2H, d, *J* = 8.70), 7.56(1H, d, *J* = 5.0), 7.49(d. 1H, *J* = 3.60), 7.41(1H, d, *J* = 15.20), 7.23–7.21(1H, m). ^{13}C-NMR(100 MHz, $CDCl_3$): 188.65, 140.25, 139.22, 137.73, 136.43, 132.40, 129.82, 129.10, 128.94, 128.42, 120.16.

(E)-1-(4-chlorophenyl)-3-(2,4-dichlorophenyl)prop-2-en-1-one (11): Yield: 70%; cream/off white crystalline solid; MP: 114–116 °C (lit. = 115–117 °C)[89]; Rf. value:0.42 (EtOAc/nhexane,1:4); FTIR (KBr, cm^1): 3085, 1675, 1610, 1530, 1490, 1275, 1035. ^{1}H-NMR(600 MHz, DMSO-d_6): 8.28(1H, d, *J* = 8.50), 8.21(2H, d, *J* = 8.60), 8.05(1H, d, *J* = 15.50), 7.99(1H, d, *J* = 15.50), 7.77(s. 1H), 7.67(2H, d, *J* = 8.60), 7.58(1H, d, *J* = 8.50). ^{13}C-NMR (150 MHz, DMSO-d_6): 187.87, 138.48, 137.63, 135.79, 135.20, 131.25, 130.57, 129.92, 129.50, 128.95, 127.96, 125.01.

(E)-1-(4-methoxyphenyl)-3-phenylprop-2-en-1-one (12): Yield: 72%; white crystalline solid; MP:106–108 °C (lit. = 104–110 °C)[80,90]; Rf. value:0.45(Ethyl acetate/n-hexane,1:4); FT-IR (KBr, cm^{-1}): 3045, 1655–1665,1605, 1550, 1135. ^{1}H-NMR(400 MHz, $CDCl_3$): 8.15(2H, d, *J* = 8.90), 7.92(1H, d, *J* = 15.60), 7.74–7.71(2H, m), 7.67(1H, d, *J* = 15.60), 7.51–7.48(3H, m), 7.07(2H, d, *J* = 8.90), 3.94(3H, s, -OCH_3). ^{13}C-NMR (100 MHz, $CDCl_3$): 188.58, 163.38, 143.68, 135.0, 131.06, 130.83, 130.35, 128.93, 128.39, 121.84, 113.85, 55.50.

(E)-3-(2-hydroxyphenyl)-1-(4-methoxyphenyl)prop-2-en-1-one (13): Yield**:** 70%; dark color solid; MP: 152–154 °C (lit. = 151–153 °C)[90]; Rf. value. 0.40 (Ethyl acetate/n-hexane,1:4);FT-IR (KBr, cm $^{-1}$): 3242, 3010, 1650, 1580, 1550, 1505, 1230, 1150. ^{1}H-NMR(400 MHz, DMSO-d_6): 8.16(2H, d, *J* = 8.90), 8.11(1H, d, *J* = 15.40), 8.07(1H, d, *J* = 15.40), 7.63(1H, d, *J* = 7.80), 7.17(2H, d, *J* = 8.90), 7.13 (1H,t, *J* = 7.0), 6.85(1H, d, *J* = 7.70), 6.56(1H, t, *J* = 6.90), 3.94(3H, s, -OCH_3). ^{13}C-NMR (100 MHz, DMSO-d_6): 188.56, 163.10, 143.35, 132.16, 132.08, 130.74, 130.47, 122.39, 119.60, 117.78, 114.30, 55.92.

(E)-3-(furan-2-yl)-1-(4-methoxyphenyl)prop-2-en-1-one (14): Yield**:** 80%; cream color crystalline solid; MP: 77–79 °C (lit. = 76–78 °C)[83]; Rf. Value. 0.40 (Ethyl acetate/n-hexane,1:4); FT-IR (KBr, cm^{-1}): 3110, 1650, 1585, 1505, 1310. ^{1}H-NMR(400 MHz, $CDCl_3$): 8.16(2H, d, *J* = 9.0), 7.71(1H, d, *J* = 15.30), 8.62(1H, d, *J* = 2.0), 7.59(1H, d, *J* = 15.30), 7.09(2H, d, *J* = 9.0), 6.81 (1H,d, *J* = 3.45), 6.62–6.61(1H, m), 3.99(3H, s, -OCH_3). ^{13}C-NMR (100 MHz, $CDCl_3$): 188.29, 163.65, 151.76, 131.05, 130.61, 130.0, 119.21, 115.77, 113.77, 112.59, 55.92.

(E)-1-(4-methoxyphenyl)-3-(3-nitrophenyl)prop-2-en-1-one (15): Yield: 70%; white solid; MP:152–154 °C (lit. = 151–152 °C)[91]; Rf. Value:0.40(Ethyl acetate/n-hexane,1:4); FT-IR (KBr, cm $^{-1}$): 3090, 1660, 1595, 1505, 1320. ^{1}H-NMR(600 MHz, $CDCl_3$): 8.52 (1H, s), 8.28(1H, d, *J* = 7.70), 8.09(2H, d, *J* = 8.80), 7.94(1H, d, *J* = 7.70), 7.85(1H, d, *J* = 15.60), 7.70(1H, d, *J* = 15.60), 7.64(1H, t, *J* = 7.90), 7.03(2H, d, *J* = 8.80), 3.92 (3H, s, -OCH_3). ^{13}C-NMR (150 MHz, $CDCl_3$): 187.87, 163.89, 148.65, 140.74, 136.94, 134.45, 131.01, 130.50, 130.03, 124.49, 122.21, 114.04, 55.66.

(E)-3-(4-(dimethylamino)phenyl)-1-(4-methoxyphenyl)prop-2-en-1-one (16): Yield**:** 65%; deep yellow crystalline solid; MP: 129–130 °C (lit. = 129–131 °C)[90,92]; Rf.value:0.40(Ethyl acetate/n-hexane,1:4); FT-IR (KBr, cm $^{-1}$): 3030, 1640, 1590, 1560, 1510, 1150,1320. ^{1}H-NMR(400 MHz, $CDCl_3$): 8.15(2H, d, *J* = 8.80), 7.921(1H, d, *J* = 15.50), 8.65(2H, d, *J* = 8.80), 7.48(1H, d, *J* = 15.50), 7.08(2H, d, *J* = 8.80), 6.78 (2H,d, *J* = 8.80), 3.95(3H, s, -OCH_3), 3.10(6H, s, -$N(CH_3)_2$. ^{13}C-NMR (100 MHz, $CDCl_3$): 188.56, 162.82, 152.04, 144.53, 131.85, 130.53, 130.29, 122.76, 116.55, 113.69, 111.83, 55.59, 39.89.

(E)-1,3-bis(4-methoxyphenyl)prop-2-en-1-one (17): Yield: 70%; white crystalline solid; MP: 99–102 °C (lit. = 100–103 °C)[80]; Rf. value: 0.4 (Ethyl acetate/n-hexane,1:4); FT-IR (KBr, cm $^{-1}$): 3050, 1655 ,1575, 1555, 1510, 1240, 1150. ^{1}H-NMR(400 MHz, $CDCl_3$): 8.15(2H, d, *J* = 8.90), 7.90(1H, d, *J* = 15.60), 7.1(2H, d, *J* = 8.70), 7.55(1H, d, *J* = 15.90), 7.09(2H, d, *J* = 8.90), 7.04 (2H,d, *J* = 8.70), 3.98(3H, s, -OCH_3), 3.94(3H, s, -OCH_3). ^{13}C-NMR (100 MHz, $CDCl_3$): 188.56, 163.38, 161.64, 143.70, 131.34, 130.69, 130.06, 127.79, 119.53, 114.38, 113.79, 55.54, 39.89.

(E)-1-(4-methoxyphenyl)-3-(p-tolyl)prop-2-en-1-one (18): Yield: 75%; white crystalline solid; MP: 124–126 °C (lit. = 127–127.5 °C)[80]; Rf. Value. 0.4(Ethyl acetate/n-hexane,1:4); FT-IR (KBr, cm $^{-1}$): 3058, 1646 ,1580, 1570, 1515, 1265, 1025 ^{1}H-NMR(400 MHz, $CDCl_3$): 8.03(2H, d, *J* = 8.90), 7.79(1H, d, *J* = 15.60), 7.53(2H, d, *J* = 8.40), 7.47(1H, d, *J* = 15.60), 7.21(2H, d, *J* = 8.40), 6.97 (2H,d, *J* = 8.90), 3.85(3H, s, -OCH_3), 2.36(3H, s, -CH_3). ^{13}C-NMR(100 MHz, $CDCl_3$): 188.58, 163.35, 143.97, 140.77, 132.34, 130.77, 129.68, 128.40, 120.85, 113.71, 55.54, 31.32.

(E)-1-(4-methoxyphenyl)-3-(3-hydroxy-4-methoxyphenyl)prop-2-en-1-one (19): Yield: 70%; yellow crystalline solid; MP: 126–128 °C (lit. = 128–130 °C)[93]; Rf. value: 0.45(Ethyl acetate/n-hexane,1:5); FT-IR (KBr, cm $^{-1}$): 3365, 3050, 1645, 1580, 1555, 1510, 1250, 1010. ^{1}H-NMR(600 MHz,DMSO-d_6): 8.09(1H, d, *J* = 15.50), 8.06(2H, d, *J* = 7.90), 7.85(1H, d, *J* = 15.50), 7.32(1H, d, *J* = 7.70), 7.07(2H, d, *J* = 7.90), 6.87(1H, d, *J* = 7.70), 6.58 (1H,s), 3.85(3H, s, -OCH_3), 3.75(3H, s, -OCH_3). ^{13}C-NMR (150 MHz, DMSO-d_6): 187.75, 162.75, 149.54, 140.53, 131.27, 130.40, 121.27, 118.62, 115.53, 113.77,112.91, 55.68, 55.44.

(E)-1-(4-methoxyphenyl)-3-(3H-pyrrol-2-yl)prop-2-en-1-one (20): Yield: 72%; deep yellow crystalline solid; MP: 168–170 °C (lit. = 168 °C)[85]; Rf. value. 0.50(Ethyl acetate/n-hexane,1:4); FT-IR(KBr, cm $^{-1}$): 3045, 1635 ,1595, 1565, 1520, 1235, 1025 ^{1}H-NMR(400 MHz, $CDCl_3$): 8.13(2H, d, *J* = 8.90), 7.86(1H, d, *J* = 15.50), 7.28(1H, d, *J* = 15.50),7.10–7.09(1H, m), 7.07(2H, d, *J* = 8.90), 6.83–6.81(1H, m), 6.46–6.43(1H, m), 4.0 (3H, s, -OCH_3). ^{13}C-NMR (100 MHz, $CDCl_3$): 188.57, 163.11, 133.73, 131.50, 130.51, 129.45, 122.72, 115.56, 114.80, 113.76, 111.40, 55.71.

(E)-1-(4-methoxyphenyl)-3-(3,4,5-trimethoxyphenyl)prop-2-en-1-one (21): Yield: 70% ; off white crystalline solid; MP: 129–130 °C (lit. = 131.1–132.5 & 129 °C)[84,87,94]; Rf. value: 0.50 (EtOAc/n-hexane,1:4); FT-IR(KBr, cm $^{-1}$): 3060, 1665, 1595, 1580, 1530, 1235, 1005. ^{1}H-NMR(400 MHz, $CDCl_3$): 8.04(2H, d, *J* = 8.80), 7.72(1H, d, *J* = 15.50), 7.44(1H, d, *J* = 15.50), 6.98(2H, d, *J* = 8.80), 6.86(2H, s), 3.91(6H, s, -2OCH_3), 3.89(3H, s, -OCH_3),

3.87(3H, s, -OCH_3). ^{13}C-NMR (100 MHz, $CDCl_3$): 188.57, 163.38, 153.34, 144.10, 140.23, 131.08, 130.78, 130.56, 121.19, 113.82, 105.57, 60.97, 56.20, 55.47.

(*E*)-1-(4-methoxyphenyl)-3-(thiophen-2-yl)prop-2-en-1-one (***22***): Yield: 70%; off white crystalline solid; MP: 107–109 °C (lit. = 104–106 °C)[83]; Rf. value: 0.43 (EtOAc/n-hexane,1:4), FT-IR (KBr, cm $^{-1}$): 3025, 1625, 1560, 1530, 1490, 1245, 1025. ^{1}H-NMR(400 MHz, $CDCl_3$): 8.13(2H, d, *J* = 8.90), 8.05(1H, d, *J* = 15.30), 7.50(1H, d, *J* = 5.0), 7.46(1H, d, *J* = 15.30), 7.42(d. 1H, *J* = 4.0), 7.18–7.16(1H, m), 7.08(2H, d, *J* = 8.90), 3.96 (3H, s, -OCH_3). ^{13}C-NMR (100 MHz, $CDCl_3$): 188.01, 163.38, 140.49, 136.37, 131.74, 130.98, 130.71, 128.48, 128.31, 120.62, 113.85, 55.48.

(E)-3-(2-chlorophenyl)-1-(4-methoxyphenyl)prop-2-en-1-one (23): Yield: 64%; white crystalline solid; MP: 131–134 °C (lit. = 135–138 °C)[95]; Rf. value: 0.38(EtOAc/n-hexane,1:4), FT-IR(KBr,cm^{-1}): 3058,1685,1580,1540 ,1500,1125,840. ^{1}H-NMR(600 MHz, DMSO-d_6): 8.21–8.20 (m, 1H), 8.19(2H, d, *J* = 8.90), 8.04(1H, d, *J* = 15.50), 7.99(1H, d, *J* = 15.50), 7.56–7.44(3H, m), 7.10(2H, d, *J* = 8.90), 3.80(s, 3H, -OCH_3). ^{13}C-NMR (150 MHz, DMSO-d_6): 187.04, 163.64, 137.70, 134.22, 132.44, 131.72, 140.44, 130.14, 129.94, 128.51, 127.60, 124.78, 114.06, 55.70.

(E)-3-(2,4-dichlorophenyl)-1-(4-methoxyphenyl)prop-2-en-1-one (24): Yield**:** 65%; white crystalline solid; MP: 152–154 °C (lit. = 155–158 °C)[95]; Rf.value:0.50 (EtOAc/n-hexane,1:4). FT-IR (KBr, cm $^{-1}$): 3090,1695,16 50,1550,1520,1230,1025. ^{1}H-NMR(400 MHz, DMSO-d_6): 8.26(1H, d, *J* = 8.60), 8.19(2H, d, *J* = 8.90), 8.05(1H, d, *J* = 15.50), 7.95(1H, d, *J* = 15.50), 7.74(s. 1H), 7.67(2H, d, *J* = 8.60), 7.55(1H, d, *J* = 8.50), 7.11(2H, d, *J* = 8.90), 3.88(s, 3H, -OCH_3). ^{13}C-NMR (100 MHz, DMSO-d_6): 187.46, 163.94, 136.92, 135.47, 131.95, 130.46, 130.24, 129.90, 128.36, 125.76, 114.60, 56.08.

(E)-1-(4-hydroxyphenyl)-3-phenylprop-2-en-1-one (25): Yield: 75%; yellow crystalline solid; MP: 118–120 °C (lit. = 120–121 °C)[90]; Rf. Value. 0.50 (Ethyl acetate/n hexane,1:4); FT-IR (KBr, cm^{-1}): 3075, 1660, 1600, 3380. ^{1}H-NMR(400 MHz, DMSO-d_6): 8.11(2H, d, *J* = 8.80), 8.01(1H, d, *J* = 15.60), 7.94–7.92(m, 2H), 7.75(1H, d, *J* = 15.60), 7.56–7.51(3H, m), 6.88(2H, d, *J* = 8.80). ^{13}C-NMR (100 MHz, DMSO-d_6): 186.84, 167.13, 142.24, 135.55, 131.83, 131.21, 130.50, 129.32, 128.99, 122.90, 116.83.

(E)-3-(furan-2-yl)-1-(4-hydroxyphenyl)prop-2-en-1-one (26): Yield: 80%; deep yellow crystalline solid; MP: 73–75 °C (lit. = 69–71 °C)[83]; Rf**.** value. 0.55(Ethyl acetate/n-hexane,1:4); FT-IR(KBr, cm^{-1}): 3385, 3050, 1655, 1620, 1550, 1440 ^{1}H-NMR(600 MHz, $CDCl_3$): 8.06(2H, d, *J* = 8.60), 7.63(1H, d, *J* = 15.30), 7.55(m, 1H), 7.50(1H, d, *J* = 15.30), 6.97(2H, d, *J* = 8.60), 6.73(1H, d, *J* = 3.40), 6.54–6.53(1H, m). ^{13}C-NMR(150 MHz, $CDCl_3$): 188.62, 160.29, 151.74, 144.87, 131.14, 130.29, 119.09, 116.10, 115.49, 112.67.

(E)-1-(4-hydroxyphenyl)-3-(3-nitrophenyl)prop-2-en-1-one (27): Yield: 65%; orange crystalline solid; MP: 181–182 °C (lit. = 180–182 °C)[96]; Rf. Value. 0.35 (Ethyl acetate/n-hexane,1:4); FT-IR (KBr, cm $^{-1}$): 3370,3080,1655, 1590, 1503, 1315. ^{1}H-NMR(600 MHz, DMSO-d6): 10.48((1H, s, -OH), 8.77 (1H, s), 8.33(1H, d, *J* = 6.20), 8.27(1H, d, *J* = 8.30), 8.16(1H, d, *J* = 14.30), 8.14(2H, d, *J* = 7.0), 7.81(1H, d, *J* = 14.30), 7.76(1H, t, *J* = 6.40), 6.92(2H, d, *J* = 7.0). ^{13}C-NMR (150 MHz, DMSO-d_6): 186.84, 167.13, 142.24, 135.55, 131.83, 131.21, 130.50, 129.32, 128.99, 122.90, 116.83.

(E)-1-(4-hydroxyphenyl)-3-(4-methoxyphenyl)prop-2-en-1-one (28): Yield: 75%; yellow crystalline solid; MP: 182 °C (lit. = 179–181 °C)[90]; Rf. value: 0.45 (Ethyl acetate/n-hexane,1:4); FT-IR (KBr,cm^{-1}): 3380,3025, 1650, 1580, 1550,3378,1160. ^{1}H-NMR(600 MHz, $CDCl_3$): 10.45(s, 1H, -OH), 8.10(2H, d, *J* = 8.0), 7.83(2H, d, *J* = 8.20), 7.78(1H, d, *J* = 15.40),7.67(2H, d, *J* = 15.40), 7.0(2H, d, *J* = 8.0), 6.93(2H, d, *J* = 8.20), 3.79(3H, s, -OCH_3). ^{13}C-NMR (150 MHz, $CDCl_3$): 187.07, 162.01, 161.06, 142.68, 131.02, 130.49, 129.32, 127.47, 119.48, 115.31, 114.30, 54.89.

(E)-1-(4-hydroxyphenyl)-3-(pyridin-2-yl)prop-2-en-1-one (29): Yield**:** 70%; cream color crystalline solid; MP: 90–92 °C (lit. = 93 °C)[86]; Rf. value: 0.38(EtOAc/n hexane,1:4); FT-IR (KBr, cm $^{-1}$): 3240, 3054, 1642, 1550, 1530, 1505, 1235, 1025. ^{1}H-NMR(600 MHz, DMSO-d_6): 8.66(2H, d, *J* = 8.60), 8.13(1H, d, *J* = 15.40), 7.88–7.85(3H ,m), 7.59(1H, d, *J* = 15.40), 7.39–7.37(1H, m), 6.60(2H, d, *J* = 8.60). ^{13}C-NMR (150 MHz, DMSO-d_6): 185.28, 171.36, 153.63, 149.83, 139.81, 136.91, 131.44, 126.61, 124.07, 117.52, 116.83.

(E)-1-(4-hydroxyphenyl)-3-(3,4,5-trimethoxyphenyl)prop-2-en-1-one (30): Yield: 70%; light yellow crystalline solid; MP: 183–185 °C (lit. = 180–182 °C)[87]; Rf. value:0.35 (EtOAc/n-hexane); FT-IR (KBr,cm^{-1}): 3260, 3024, 1637, 1575, 1555, 1520, 1257, 1025. ^{1}H-NMR(400 MHz, $CDCl_3$): 8.01(2H, d, *J* = 8.50), 7.69(1H, d, *J* = 15.50), 7.40(1H, d, *J* = 15.50), 6.95(2H, d, *J* = 8.50), 6.81(2H, s), 3.87(6H, s, -$(OCH_3)_2$), 3.85(3H, s, -OCH_3). ^{13}C-NMR (100 MHz, $CDCl_3$): 188.59, 163.39, 153.50, 144.26, 130.89, 121.08, 105.08, 61.05, 56.25, 55.52.

(E)-1-(4-hydroxyphenyl)-3-(thiophen-2-yl)prop-2-en-1-one (31): Yield: 67%; deep yellow crystalline solid; MP: 150–152 °C (lit. = 154–156 °C)[83]; Rf. value: 0.35 (EtOAc/nhexane,1:4); FT-IR (KBr, cm $^{-1}$): 3024, 1705,1690,1460,1410,1355, 1045. ^{1}H-NMR(600 MHz, DMSO-d_6): 8.0(2H, d, *J* = 8.70), 7.85(1H, d, *J* = 15.20), 7.72(1H, d, *J* = 5.0), 7.62(1H, d, *J* = 3.40), 7.54(1H, d, *J* = 15.20), 7.17–7.16(1H, m), 6.90(2H, d, *J* = 8.70). ^{13}C-NMR (150 MHz, DMSO-d_6): 186.78, 161.89, 139.92, 135.56, 132.32, 131.02, 129.91, 128.86, 128.69, 120.24,115.14.

(E)-3-(2,4-dichlorophenyl)-1-(4-hydroxyphenyl)prop-2-en-1-one (32): Yield**:** 62%; deep yellow crystalline solid; MP: 116–117 °C (lit. = 120–121 °C)[89]; Rf. Value. 0.42 (EtOAc/n-hexane,1:4); FT IR (KBr, cm^1):3175,3065, 1695,1560,1530,1480,1235,1045. ^{1}H-NMR(600 MHz, $CDCl_3$): 7.94 (1H, d, *J* = 15.7 Hz), 7.84 (2H, d, *J* = 8.3 Hz), 7.60 (1H, d, *J* = 8.4 Hz), 7.40 (1H, d, *J* = 15.7 Hz), 7.35 (1H. s), 7.19 (1H, d, *J* = 8.3 Hz), 6.80 (2H, d, *J* = 8.2 Hz).^{13}C-NMR(150 MHz, $CDCl_3$): 188.96, 162.30, 138.36, 136.21, 135.82, 131.94, 131.27, 129.95, 129.41, 128.52, 127.49, 125.03, 115.50.

(E)-3-(4-hydroxy-3-methoxyphenyl)-1-phenylprop-2-en-1-one (33): Yield: 70%; dark brown crystalline solid; MP: 117–118 °C (lit. = liquid)[33]; Rf. value: 0.45 (Ethyl acetate/n-hexane,1:4); IR (KBr, cm $^{-1}$): 3023, 1655, 1595, 1570, 1515, 1265, 1020. ^{1}H-NMR(600 MHz, DMSO-d_6): 8.07(1H, d, *J* = 14.90), 7.94(2H, d, *J* = 7.80), 7.78(1H, d, *J* = 14.90), 7.55–7.44(3H, m), 6.87(1H, d, *J* = 7.80), 6.42(1H, d, *J* = 6.72), 5.85(1H, s), 3.62(3H, s, -OCH_3). ^{13}C-NMR (150 MHz, DMSO-d_6): 189.08, 153.38, 146.62, 140.55, 131.12, 128.25, 127.56, 120.97, 111.44, 106.25, 55.06.

(E)-1-phenyl-3-(3H-pyrrol-2-yl)prop-2-en-1-one (34): Yield:73%; deep yellow crystalline solid; MP: 131–133 °C (lit. = 130 °C)[85];Rf. value:0.50(Ethylacetate/n-hexane,1:4);FT-IR(KBr,cm^{-1}):3056,1642,1595,1565,1525,1260,1020 ^{1}H-NMR(400 MHz, DMSO-d_6): 11.81(1H, s), 8.13–8.11(2H, m), 7.73–7.64(5H, m), 7.25–7,23(1H, m), 6.84–6.82(1H, m), 6.33–6.31(1H, m). ^{13}C-NMR (100 MHz, DMSO-d_6): 188.83, 138.81, 134.76, 133.16, 129.58, 128.38, 124.78, 116.88, 115.05, 111.14.

(E)-1-phenyl-3-(3,4,5-trimethoxyphenyl)prop-2-en-1-one (35): Yield: 72%; off white crystalline solid; MP: 118–120 °C (lit. = 120–122 °C)[87]; Rf. value:0.40 (Ethylacetate/n-hexane,1:4); FT-IR (KBr,cm^{-1}): 3034, 1635, 1570, 1550, 1525, 1275, 1025. ^{1}H-NMR(600 MHz, DMSO-d_6): 8.04–8.02(2H, m), 7.75(1H, d, *J* = 15.60), 7.62–7.52(3H, m), 7.43(1H, d, J = 15.60), 6.89(2H, s), 3.44(6H, s, 2-OCH_3), 3.43(3H, s, -OCH_3). ^{13}C-NMR (150 MHz, DMSO-d_6): 190.76, 153.62, 144.83, 140.68, 138.35, 132.82, 130.50, 128.39, 121.71, 105.57, 60.83, 56.40.

(E)-3-(4-(dimethylamino)phenyl)-1-phenylprop-2-en-1-one (36): Yield: 78%; orange/deep yellow color crystalline solid; MP: 110–112 °C (lit. = 111–113 °C[96]; Rf. Value: 0.50(Ethylacetate/nhexane,1:4); FTIR (KBr, cm^{1}): 3015, 1667, 1560, 1330. ^{1}H-NMR(400 MHz, $CDCl_3$): 8.12(2H, d, *J* = 5.60), 7.93(1H, d, J = 15.0), 7.65–7.60(5H, m), 7.47(1H, d, J = 15.0), 6.81(2H, d, *J* = 5.60), 3.14(6H, s, -$N(CH_3)_2$. ^{13}C-NMR (100 MHz, $CDCl_3$): 190.93, 152.06, 145.71, 129.03, 132.35, 130.62, 128.32, 122.82, 116.98, 112.03, 40.45.

(E)-1-phenyl-3-(p-tolyl)prop-2-en-1-one (37): Yield: 75%; white crystalline solid; MP: 92–94 °C (lit. = 94–96 °C)[80]; Rf. Value: 0.5 (Ethyl acetate/n-hexane,1:4); FT-IR (KBr, cm^{-1}): 3040, 1650,1580, 1550, 1520, 1265, 1020. ^{1}H-NMR(40 MHz, $CDCl_3$): 8.15(2H, d, *J* = 7.0), 7.94(1H, d, J = 15.70), 7.67–7.59(6H, m), 7.34(2H, d, J = 7.70), 2.50(3H, s, -CH_3). ^{13}C-NMR(100 MHz, $CDCl_3$): 190.65, 145.08, 141.05, 138.48, 132.70, 132.20, 129.76, 128.61, 128.52, 128.49,121.08, 21.56.

(E)-1-(thiophen-2-yl)-3-(3,4,5-trimethoxyphenyl)prop-2-en-1-one (38): Yield: 88%; white crystalline solid; MP: 146–148 °C (lit. = 147–148 °C)[97]; Rf. Value: 0.5 (Ethyl acetate/n-hexane,1:5); FT-IR (KBr, cm^{-1}): 3038, 1651,1578, 1548, 1521, 1266, 1022. ^{1}H-NMR(400 MHz, $CDCl_3$): 7.89–7.87(1H, m), 7.78(1H, d, J = 15.50), 7.69–7.67(1H, m), 7.32(1H, d, J = 15.50), 7.19–7.17(1H, m), 6.86(2H, s), 3.92(6H, s, -2OCH_3). 3.90(3H, s, -OCH_3). ^{13}C-NMR (100 MHz, $CDCl_3$): 190.65, 145.08, 141.05, 138.48, 132.70, 132.20, 129.76, 128.61, 128.52, 128.49,121.08, 21.56.

(E)-3-(4-methoxyphenyl)-1-(thiophen-2-yl)prop-2-en-1-one (39): Yield: 90%; white crystalline solid; MP: 69–69 °C (lit. = 68 °C)[98]; Rf. Value: 0.50 (Ethyl acetate/n-hexane,1:4); FT-IR (KBr, cm^{-1}): 3040, 1652,1576, 1547, 1520, 1265, 1021. ^{1}H-NMR(400 MHz, $CDCl_3$): 7.85–7.83(1H, m), 7.65–7.64(1H, m), 7.79(1H, d, J = 15.50), 7.60(2H, d, J = 8.50), 7.32(1H, d, J = 15.50), 7.17–7.15(1H, m), 6.93(2H, d, *J* = 8.50), 3.84(3H, s, -OCH_3). ^{13}C-NMR (100 MHz, $CDCl_3$): 181.95, 161.92, 145.98, 143.97, 133.83, 131.54, 130.28, 128.16, 127.46, 119.29,114.44, 55.65.

(E)-3-(4-chlorophenyl)-1-(thiophen-2-yl)prop-2-en-1-one (40): Yield: 90%; white crystalline solid; MP: 126–127 °C (lit. = 128 °C)[98]; Rf. Value: 0.50 (Ethyl acetate/n-hexane,1:4); FT-IR (KBr, cm^{-1}): 3040, 1650, 1570, 1545, 1525, 1260, 1020. ^{1}H-NMR(400 MHz, $CDCl_3$): 7.86–7.85(1H, m), 7.79(1H, d, *J* = 15.60), 7.68–7.67(1H, m), 7.56(2H, d, J = 8.48), 7.39(1H, d, J = 15.60), 7.36(1H, d, J = 15.60), 7.18–7.16(1H, m), 6.93(2H, d, *J* = 8.48). ^{13}C-NMR (100 MHz, $CDCl_3$): 181.98, 145.05, 142.54, 136.49, 133.17, 131.92, 129.64, 129.25, 128.33, 122.05.

In vitro α-amylase inhibition protocol

The structurally characterized chalcones (**1–40**) were investigated against α-amylase enzyme via a previously reported protocol with little modification[99], which involves the addition of 20 µl of dimethyl sulfoxide (DMSO) to each well, then twenty microliters of each sample was added, subsequently 50 µl of PBS (PH = 6.8) was added to each respective well. Afterward, 20 µL of starch was added to each well, and the mixture was incubated for 20 min at 37 °C. In the next step, 10 µL of the α-amylase enzyme was introduced into a separate well. At the end, 100 µL of dinitrosalicylic acid (DNS) was added to a separate well and incubated for 30 min at 37 °C. Finally, absorbance was measured at 540 nm by using a Biotech microplate reader, and acarbose was used as a standard at different concentrations. All the experiments were conducted in triplicate[99]. At the end, the obtained results were expressed in IC_{50} by using GraphPad Prism software.

In vitro DPPH protocol

The antioxidant activity of the synthesized chalcone series was measured using the DPPH free radical scavenging assay, as previously reported with minor modifications[100,101]. The investigation was conducted by adding 100 µL of each tested sample, dissolved in dimethyl sulfoxide (DMSO), to a 96-well plate. Afterward, an equal volume of DPPH (100 mM) dissolved in methanol was charged to the separate sample. Then, incubated for 30 min at ambient temperature in the absence of light, and ascorbic acid was applied as a standard. All the experiments were conducted in triplicate[100]. Lastly, the investigation was conducted by measuring their IC_{50} values via absorbance at 517 nm through a Biotech microplate reader.

Computational methods

Protein preparation

The X-ray structure of human pancreatic α-amylase (PDB ID: 1B2Y)[102] was imported into the Maestro workspace v.9.3 (Schrödinger, LCC, New York, 2012) and prepared using Protein Preparation Wizard. In this step, hydrogen atoms were added, and bond orders and formal charges were adjusted accordingly. The Epik[103] was employed to predict the protonation states (pK_a) of polar amino acids at pH 7.4 ± 0.5, whereas PROPKA v.3.1[104] was used to optimize hydrogen orientations. Missing loop regions were reconstructed using Prime's loop refinement under the OPLS2005 force field[105].

Conformer generation

To account for protein flexibility, a pool of conformations was generated using CABS-flex 3.0, a coarse-grained molecular dynamics simulation tool[106]. It allows efficient exploration of conformational space while maintaining computational efficiency. Simulations were performed using default parameters, with particular attention to

the flexible loops surrounding the catalytic site. Four representative conformations were selected by aligning all generated models to the crystallographic reference. Special attention was given to selecting conformations that displayed significant differences in active-site geometry, ensuring adequate sampling of the conformational landscape of the substrate-binding groove.

Benchmark dataset

A curated dataset of 189 known α-amylase inhibitors ($IC_{50} \leq 20$ μM) was extracted from the ChEMBL database (CHEMBL6066863). For each active compound, 36 property-matched decoys (6,804 compounds) were generated using the LUDe (Ligand Unbiased Decoys) server[107], that maintain similar physicochemical properties while ensuring topological dissimilarity. All actives and decoys were imported into the Maestro workspace v.9.3 and prepared using LigPrep v.2.5 (Schrödinger, LLC) at a pH of 7.4 ± 0.5, followed by geometric optimization using OPLS2005.

Molecular docking protocol

A receptor grid was generated for each protein conformation using the Receptor Grid Generation panel in Glide v.5.8. The grid center was defined based on the acarbose binding site in the co-crystal structure (coordinates: x = 37.64 Å, y = -25.58 Å, z = -49.06 Å). The outer box was set to 20 Å to encompass the entire substrate-binding groove spanning pockets -3 to + 2. The inner box, defining the ligand center-of-mass sampling region, was set to 10 Å. Molecular docking calculations were performed using Glide v.5.8 in Standard Precision (SP) mode, with flexible ligand sampling and Epik state penalties applied. Poses were scored using the Docking Score empirical function, which integrates Van der Waals and electrostatic interaction terms, hydrogen-bond rewards, lipophilic complementarity, and Epik-derived ionization-state penalties. Each compound in the benchmark dataset was docked independently against all five protein conformations, yielding a comprehensive ensemble protocol. The docking results were then aggregated by extracting 18 intermolecular descriptors (i.e., scores, energy terms) per conformation. Additionally, to assess pose reliability, redocking experiments were performed using co-crystallized acarbose. Root-mean-square deviation (RMSD) was calculated for heavy atoms to assess pose reproduction accuracy, with RMSD < 2.0 Å considered successful.

Machine learning re-scoring

To improve the discrimination between actives and decoys beyond conventional Docking Scores, the aggregated ensemble docking dataset was analyzed in KNIME v.5.2.5 to derive a Bayesian scoring function. In this context, docking-derived energy terms and scoring functions were used as intermolecular descriptors. The most informative variables were then selected using a genetic algorithm, and a Naive Bayes classifier was trained under fivefold cross-validation. Model performance was evaluated using Enrichment Factor at 1% ($EF_{1\%}$), Boltzmann-Enhanced Discrimination of Receiver Operating Characteristic at 1% ($BEDROC_{1\%}$, α = 20), and Area Under the ROC curve (AUROC).

In silico ADMET analysis

ADMETLab v.3.0[108] was used to predict key drug-like properties and the ADMET profile of the top synthesized hits. The analysis included physicochemical descriptors, namely logS, logD, and logP, which inform aqueous solubility, pH-dependent distribution behavior, and intrinsic lipophilicity, respectively. Absorption-related parameters were also evaluated, including Caco-2 permeability and the parallel artificial membrane permeability assay (PAMPA) for blood–brain barrier permeation. Metabolism-related properties were also examined, including human liver microsome (HLM) stability. Elimination markers included plasma clearance (CLplasma). Toxicity endpoints included human ether-à-go-go-related gene (hERG) channel blockade, drug-induced liver injury (DILI) hepatotoxicity, and Ames mutagenicity.

Results and discussion

Synthesis and structural characterization

In this work, we synthesized a series of 40 chalcone analogs (compounds **1**–**40**, Table 1) through a Claisen–Schmidt condensation. The compounds were obtained by base-promoted coupling of appropriately substituted aromatic aldehydes with acetophenone derivatives at room temperature, as outlined in Fig. 2. The substitution pattern was designed to sample electron-donating, electron-withdrawing, hydrogen-bonding, and heteroaryl environments, thereby enabling an initial assessment of how electronic and pharmacophoric features influence the biological profile of the chalcone scaffold. For clarity, the synthesized chalcones were organized into five series according to the substitution pattern of ring A. In the first series (**1–11**), second (**12–24**), third (**25–32**), fourth (**33–37**), and fifth (**38–40**) series, *p*-chlorophenyl, *p*-methoxyphenyl, *p*-hydroxyphenyl, phenyl, and thiophene were used as ring A, respectively, while different substituted benzene were used as ring B. Reaction progress was monitored by TLC, and the crude products were purified through recrystallization from ethanol, yielding amounts between 64 and 90%.

The structural characterization of the synthesized analogs was then performed by FT-IR and $^{1}H/^{13}C$ NMR spectroscopy. In the FT-IR spectra, the chalcone derivatives displayed the expected absorptions associated with aromatic C–H stretching (3090–3010 cm^{-1}), olefinic C–H (1600–1650 cm^{-1}), and conjugated enone carbonyl group (1690–1650 cm^{-1}). Furthermore, the ^{1}H-NMR spectra of the synthesized compounds were recorded in deuterated solvents such as DMSO and chloroform on 600- and 400-MHz NMR spectrometers. Interestingly, all characterized compounds exhibit characteristic peaks of the trans-chalcone scaffold which lies in the range of 8.00 to 7.00 ppm, with large coupling constants of around 15–19 Hz.

In addition, peaks for various substituted benzene rings were found in the aromatic range. Similarly, singlet peaks for different substituents, such as methoxy, methyl, and dimethylamino groups, were observed at 3.80–

Code of compd	Ring A	Ring B	α-Amylase IC_{50} (μM ± SD)	DPPH IC_{50} (μM ± SD)
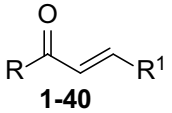 **1-40**				
1	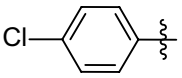	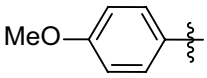	48.03 ± 2.78	75.97 ± 0.90
2	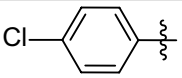	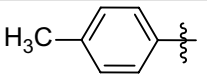	37.15 ± 0.30	211.23 ± 0.68
3	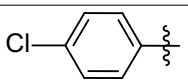	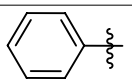	49.03 ± 0.89	264.07 ± 0.11
4	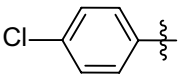	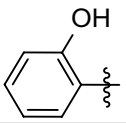	10.41 ± 1.23	237.06 ± 0.07
5	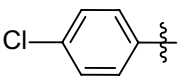	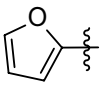	21.24 ± 0.63	135.51 ± 2.70
6	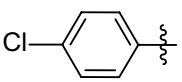	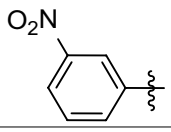	92.21 ± 3.57	117.62 ± 1.40
7	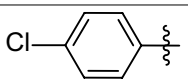	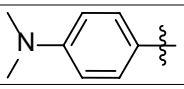	32.34 ± 2.95	47.34 ± 1.18
8	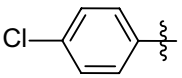	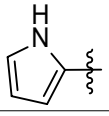	587.44 ± 6.71	365.63 ± 0.43
9	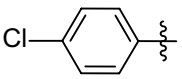	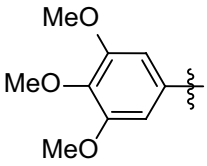	38.11 ± 2.90	120.57 ± 0.46
10	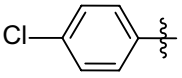	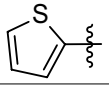	393.51 ± 5.86	698.34 ± 14.56
11	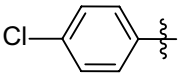	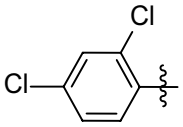	194.10 ± 6.61	158.79 ± 4.24
12	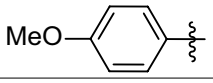	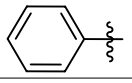	174.21 ± 0.64	180.54 ± 0.18
13	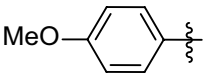	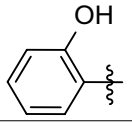	117.21 ± 4.45	199.81 ± 0.07
14	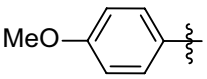	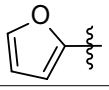	104.14 ± 0.73	113.87 ± 0.72

Continued

Code of compd	Ring A	Ring B	α-Amylase IC_{50} (μM ± SD)	DPPH IC_{50} (μM ± SD)
	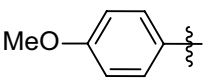	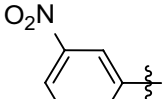		
15			51.32 ± 1.97	229.66 ± 0.31
16	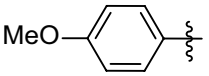	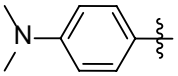	32.13 ± 3.38	56.33 ± 0.44
17	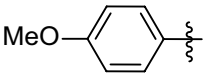	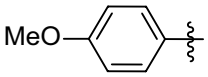	23.07 ± 0.55	99.17 ± 0.40
18	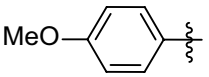	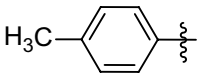	26.60 ± 0.98	56.87 ± 0.36
19	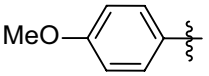	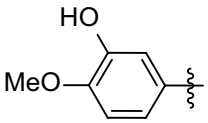	15.44 ± 0.29	202.80 ± 0.64
20	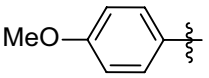	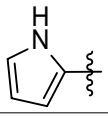	187.14 ± 0.95	340.79 ± 0.13
21	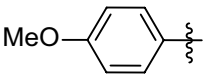	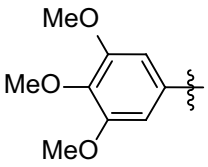	86.49 ± 0.55	92.45 ± 2.00
22	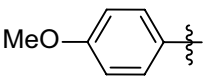	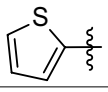	57.67 ± 0.30	207.60 ± 14.38
23	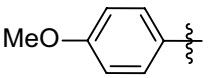	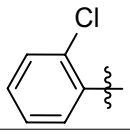	277.11 ± 3.18	359.25 ± 1.75
24	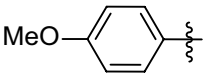	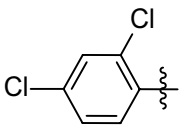	365.27 ± 3.74	261.28 ± 1.14
25	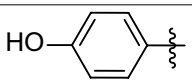	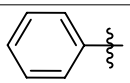	64.83 ± 0.28	198.30 ± 0.23
26	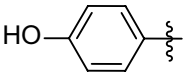	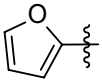	26.19 ± 1.72	63.44 ± 0.29
27	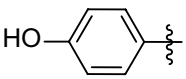	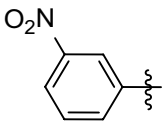	27.33 ± 4.67	266.51 ± 1.19
28	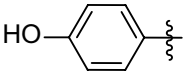	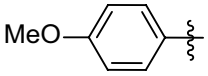	65.12 ± 2.68	240.79 ± 0.99
29	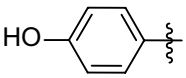	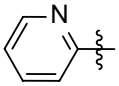	374.08 ± 1.91	299.36 ± 1.16

Continued

Code of compd	Ring A	Ring B	α-Amylase IC_{50} (μM ± SD)	DPPH IC_{50} (μM ± SD)
	R	^{1}R		
30	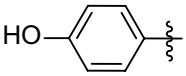	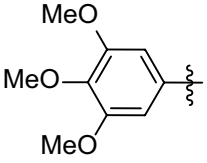	39.03 ± 0.50	49.12 ± 0.53
31	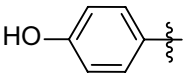	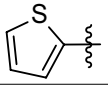	19.46 ± 0.03	99.70 ± 0.43
32	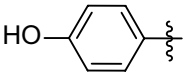	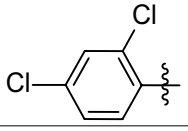	218.35 ± 10.09	290.98 ± 6.70
33	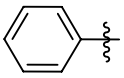	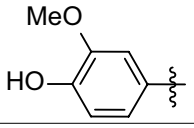	16.54 ± 0.25	227.46 ± 0.02
34	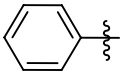	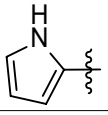	1021.64 ± 2.75	316.78 ± 0.70
35	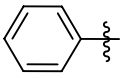	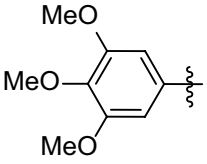	31.97 ± 1.05	31.34 ± 0.20
36	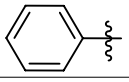	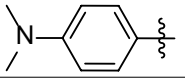	61.27 ± 1.37	219.95 ± 1.34
37	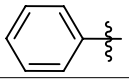	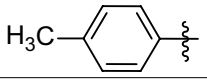	152.67 ± 2.92	192.96 ± 0.10
38	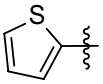	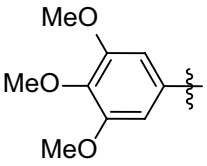	87.24 ± 2.67	118.52 ± 3.39
39	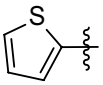	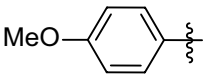	65.41 ± 1.33	201.50 ± 10.39
40	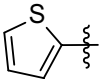	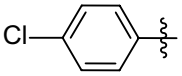	380.14 ± 6.71	675.12 ± 10.46
Standard	Acarbose		73.12 ± 5.04	------
Standard	Ascorbic acid		-------	287.30 ± 4.00

Table 1. Synthetic Chalcone derivatives (**1–40**).

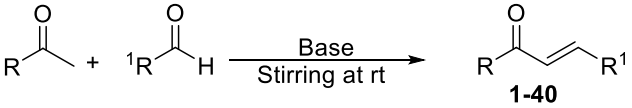

Fig. 2. Representative scheme for synthesizing chalcone analogs.

3.70 ppm, 2.80–2.70 ppm, and around 3.00 ppm, respectively. Likewise, ^{13}C-NMR recorded spectra show that the peaks in the range such as 190–188 ppm is due to carbonyl carbon, whereas various peaks in the range of 140–110 ppm are due to various aryl carbons, while peaks in the range of 80–50 ppm, are because of carbon in various substituents such as methoxy-, dimethylamino-, methyl- attached to aryl groups in chalcone derivatives. In short, all these spectroscopic data collectively confirm the presence of the said nucleus-containing compounds and are in good agreement with the literature.

α-amylase inhibition

All synthesized analogs (**1–40**) were evaluated for their α-amylase inhibitory activity, with IC_{50} values ranging from 10.41 ± 1.23 to 1021.64 ± 2.75 μM. Among them, compounds **4** (IC_{50} = 10.41 ± 1.23 μM), **19** (IC_{50} = 15.44 ± 0.29 μM), **33** (IC_{50} = 16.54 ± 0.25 μM), **31** (IC_{50} = 19.46 ± 0.03 μM), and **5** (IC_{50} = 21.24 ± 0.63 μM) emerged as the most potent members of the series, showing markedly stronger inhibition than the reference drug acarbose (IC_{50} = 73.12 ± 5.04 μM). Additional highly active analogs, including **17** (IC_{50} = 23.07 ± 0.55 μM), **26** (IC_{50} = 26.19 ± 1.72 μM), **18** (IC_{50} = 26.60 ± 0.98 μM), and **27** (IC_{50} = 27.33 ± 4.67 μM), further defined a consistent cluster of sub-30 μM inhibitors, highlighting the chalcone scaffold as a promising chemotype for α-amylase inhibition.

From a structure–activity relationship (SAR) perspective, α-amylase inhibition was strongly modulated by the substitution pattern on both aromatic termini of the chalcone scaffold. Within the 4-chlorophenyl series (**1–11**), the most pronounced gain in potency was observed for the 2-hydroxyphenyl analog **4**, indicating that introduction of an ortho-hydroxyl group on ring B is particularly favorable in this background. Good activity was also retained for the furan-2-yl derivative **5**, as well as for electron-rich aryl substituents such as 4-dimethylaminophenyl, **7** (IC_{50} = 32.34 ± 2.95 μM), 4-methoxyphenyl **1** (IC_{50} = 48.03 ± 2.78 μM), *p*-tolyl, **2** (IC_{50} = 37.15 ± 0.30 μM), and 3,4,5-trimethoxyphenyl, **9** (IC_{50} = 38.11 ± 2.90 μM), whereas potency dropped markedly for the 3-nitrophenyl, **6** (IC_{50} = 92.21 ± 3.57 μM), 2,4-dichlorophenyl, **11** (IC_{50} = 194.10 ± 6.61 μM), pyrrolyl **8** (IC_{50} = 587.44 ± 6.71 μM), and thiophenyl, **10** (IC_{50} = 393.51 ± 5.86 μM) congeners.

In the 4-methoxyphenyl subseries (**12–24**), the most favorable profiles were associated with electron-rich ring B motifs, particularly 3-hydroxy-4-methoxyphenyl, **19**(C_{50} = 15.44 ± 0.29 μM), 4-methoxyphenyl,**17** (IC_{50} = 23.07 ± 0.55 μM), *p*-tolyl, **18** (IC_{50} = 26.60 ± 0.98 μM), and 4-dimethylaminophenyl, **16** (IC_{50} = 32.13 ± 3.38 μM), whereas halogenated aryl groups such as 2-chlorophenyl, **23**(IC_{50} = 277.11 ± 3.18 μM) and 2,4-dichlorophenyl,**24**(IC_{50} = 365.27 ± 3.74 μM) were clearly detrimental.

A distinct but still favorable pattern emerged in the 4-hydroxyphenyl series (**25–32**), where heteroaryl replacements became more productive, as illustrated by the potent furan-2-yl, **26** (IC_{50} = 26.19 ± 1.72 μM) and thiophen-2-yl, **31** (IC_{50} = 19.46 ± 0.03 μM) analogs, while the 3-nitrophenyl derivative, **27** (IC_{50} = 27.33 ± 4.67 μM) also remained highly active in this context. In the unsubstituted phenyl series (**33–37**), the best activities were again associated with oxygenated ring B substituents, with 3-hydroxy-4-methoxyphenyl, **33** (IC_{50} = 16.54 ± 0.25 μM) and 3,4,5-trimethoxyphenyl,**35**(IC_{50} = 31.97 ± 1.05 uM) standing out, whereas the pyrrolyl analog **34** (IC_{50} = 1021.64 ± 2.75 μM) showed a dramatic loss of potency.

These data suggest that potent α-amylase inhibition in this series is favored by a balanced combination of aromatic complementarity and well-positioned hydrogen-bonding functionality on ring B, particularly ortho-hydroxyl and methoxy/hydroxyl-rich aryl motifs, whereas excessive halogenation and some heteroaryl replacements are generally less tolerated.

Antioxidant potential

Chalcone analogs were further evaluated for their DPPH radical-scavenging activity, revealing a broad range of activity, with IC_{50} values spanning 31.34 ± 0.20–698.34 ± 14.56 μM. The most potent compound in the series was **35** (IC_{50} = 31.34 ± 0.20 μM), followed by **7** (IC_{50} = 47.34 ± 1.18 μM), **30** (IC_{50} = 49.12 ± 0.53 μM), **16** (IC_{50} = 56.33 ± 0.44 μM), **18** (IC_{50} = 56.87 ± 0.36 μM), and **26** (IC_{50} = 63.44 ± 0.29 μM). Additional active analogs, including **1** (IC_{50} = 75.97 ± 0.90 μM), **21** (IC_{50} = 92.45 ± 2.00 μM), **17** (IC_{50} = 99.17 ± 0.40 μM), and **31** (IC_{50} = 99.70 ± 0.43 μM), further support the ability of this chalcone series to deliver consistent radical-scavenging activity. Notably, 80% derivatives displayed stronger activity than the reference antioxidant ascorbic acid (IC_{50} = 287.30 ± 4.00 μM).

From a SAR standpoint, the DPPH data indicate that radical-scavenging activity is generally favored by electron-rich substitution patterns, particularly when ring B bears dimethylamino- or methoxy-substituted aryl groups. In the 4-chlorophenyl series (**1–11**), the 4-dimethylaminophenyl derivative, **7**(IC_{50} = 47.34 ± 1.18 μM) emerged as the most active member, while 4-methoxyphenyl,**1**(IC_{50} = 75.97 ± 0.90 μM) and 3,4,5-trimethoxyphenyl,**9**(IC_{50} = 120.57 ± 0.46 μM) also retained good activity. By contrast, replacement with pyrrolyl, **8** (IC_{50} = 365.63 ± 0.43 μM) or thiophen-2-yl, **10** (IC_{50} = 698.34 ± 14.56 μM) resulted in a pronounced loss of potency.

A similar trend was observed in the 4-methoxyphenyl subseries (**12–24**), in which the most favorable profiles were associated with 4-dimethylaminophenyl, **16** (IC_{50} = 56.33 ± 0.44 μM), *p*-tolyl, **18** (IC_{50} = 56.87 ± 0.36 μM), 4-methoxyphenyl, **17** (IC_{50} = 99.17 ± 0.40 μM), and 3,4,5-trimethoxyphenyl, **21** (IC_{50} = 92.45 ± 2.00 μM) motifs, whereas halogenated aryl substituents, such as 2-chlorophenyl,**23**(IC_{50} = 359.25 ± 1.75 μM) and 2,4-dichlorophenyl, **24** (IC_{50} = 261.28 ± 1.14 μM) were clearly detrimental. In the 4-hydroxyphenyl series (**25–32**), the best activities were observed for the 3,4,5-trimethoxyphenyl analog **30** (IC_{50} = 49.12 ± 0.53 μM) and the furan-2-yl derivative **26** (IC_{50} = 63.44 ± 0.29 μM), while 3-nitrophenyl, **27** (IC_{50} = 266.51 ± 1.19 μM), 2-pyridyl, **29** (IC_{50} = 299.36 ± 1.16 μM), and 2,4-dichlorophenyl, **32** (IC_{50} = 290.98 ± 6.70 μM) were less favorable.

In the unsubstituted phenyl series (**33–37**), the superior activity of **35** (IC_{50} = 31.34 ± 0.20 μM) highlights the strong beneficial effect of a trimethoxy-substituted ring B, whereas the pyrrolyl analog **34** (IC_{50} = 316.78 ± 0.70 μM)

was among the least active compounds in the entire set. Overall, these results indicate that DPPH radical scavenging in this series is primarily driven by electron-donating substituents that stabilize the radical. In addition, the structural requirements for antioxidant activity partially overlap with those for α-amylase inhibition.

Molecular docking

To enhance our understanding of the experimental SAR trends, we conducted molecular docking simulations in the α-amylase catalytic site. Initially, molecular docking calculations were performed against the crystallographic structure of α-amylase (PDB ID: 1B2Y)[102] using the standard Docking Score function. To assess the prospective utility of this protocol for ligand prioritization, its enrichment performance was evaluated on a benchmarking set comprising 189 known α-amylase inhibitors and 6,804 property-matched decoys. Under these conditions, the docking workflow showed poor discriminatory power, yielding an AUROC of 0.40, $EF_1\%$ of 1.15, and $BEDROC_1\%$ of 0.04, indicating limited ability to distinguish active ligands from decoys (Fig. 3a). This result reflects a common limitation of conventional docking, where empirical scoring functions often poorly correlate with experimental binding affinity[109].

Subsequently, a genetic algorithm was used to select the most informative descriptors from the raw docking scores and individual energy terms, which were then used to build a Naive Bayes-based rescoring function. This machine learning approach substantially improved discrimination, achieving an AUROC of 0.75, an $EF_1\%$ of 19.25, and a $BEDROC_{1\%}$ of 0.71 (Fig. 3b). Additional gains were achieved after the incorporation of four representative α-amylase conformations generated by CABS-flex[106] into an ensemble docking scheme. These conformations were selected to represent structurally diverse states of the binding site, thereby broadening the conformational space sampled during docking. Under this refined protocol, the enrichment metrics further improved to an AUROC of 0.80, an $EF_1\%$ of 22.13, and a $BEDROC_1\%$ of 0.78 (Fig. 3b), indicating that explicit treatment of protein flexibility enhanced active–decoy discrimination. Notably, the genetic algorithm selected the Coulomb energy term, ligand efficiency, and rotatable-bond penalty among the docking-derived descriptors used for Naive Bayes training. This pattern suggests that α-amylase recognition is governed by electrostatic complementarity, size-efficient binding, and limited conformational strain. Accordingly, the ensemble docking framework was selected for the subsequent binding-mode analysis of the most active chalcone analogs.

The docking protocol was further validated by re-docking acarbose, a well-characterized α-amylase inhibitor. The predicted binding pose showed excellent agreement with the crystallographic structure, with an RMSD of 1.3 Å and preservation of key interactions within the enzyme's pockets (Fig. 3d). Acarbose occupied the -3 to + 2 pockets of the active site, establishing critical hydrogen bonds with catalytic residues (Asp197, Glu233, and Asp300) that serve as pharmacophoric anchors for inhibitor design (Fig. 3e).

Structural insights for α-amylase inhibition

After confirming the reliability of the docking setup, detailed inspection of the predicted binding poses was performed to characterize how the four most potent chalcone derivatives, **4** ($IC_{50} = 10.41 \pm 1.23$ μM); **19** ($C_{50} = 15.44 \pm 0.29$ μM); **33** ($IC_{50} = 16.54 \pm 0.25$ μM); and **31** ($IC_{50} = 19.46 \pm 0.03$ μM), interact with key residues in the *α*-amylase catalytic pocket. As shown in Fig. 3d, 4 adopted a favorable orientation spanning the -1 and + 1 pockets, with the 2'-hydroxyl performing a hydrogen bond to Glu233, while the *α,β*-unsaturated carbonyl forms a hydrogen bond with Arg195. These interactions with catalytic residue Glu233 suggest direct interference with the enzyme's hydrolytic mechanism.

Compound **19** also adopted a favorable orientation spanning the − 1 and + 1 pockets (Fig. 3g), closely resembling the binding mode observed for **4**. In this pose, the 2′-hydroxyl forms a hydrogen bond with Glu233, whereas the α,β-unsaturated carbonyl is anchored by a hydrogen bond with Arg195, supporting productive recognition of the catalytic groove. Similarly, compound **31** demonstrated π-π stacking interactions with both His201 and Tyr62, complemented by a hydrogen bond with Lys200 (Fig. 3h). The engagement of multiple aromatic residues suggests enhanced binding affinity through cooperative hydrophobic and π-electron interactions. Compound **33** maintained the conserved π-π stacking interaction with His201 while its carbonyl forms a hydrogen bond with Arg195 (Fig. 3i).

These binding mode analyses reveal that the chalcone derivatives exploit both the catalytic machinery and the extended substrate-binding groove of *α*-amylase, with the aromatic stacking interactions with His201 emerging as a conserved pharmacophoric element. Critically, compound **4** distinguishes itself by directly engaging Glu233, the key acid/base catalyst within α-amylase's catalytic site (comprising the catalytic residues Asp197, Glu233, and Asp300). This strategic interaction with the catalytic machinery, rather than the peripheral binding sites favored by compounds **19**, **31**, and **33**, provides a compelling mechanistic explanation for compound **4**'s superior inhibitory profile.

In silico ADMET analyses

In silico ADMET profiling was performed with ADMETLab v.3.0[108] to assess the developability of the prioritized chalcone derivatives. All four compounds satisfied Lipinski's Rule of Five and Veber's oral bioavailability criteria, supporting their overall drug-like character. The predicted physicochemical profiles were also favorable, with adequate aqueous solubility (logS = − 4.41 to − 2.61) and balanced lipophilicity (logD = 2.00–3.42; logP = 2.21–3.75) (Table 2). Compounds **4**, **31**, and **33** showed good Caco-2 permeability (> − 5.15 log cm/s), whereas **19** displayed a borderline value. Overall, the set remained compatible with acceptable membrane permeation. In addition, all four compounds showed moderate predicted human liver microsomal stability (instability probability = 0.30–0.61) and intermediate plasma clearance (7.53–11.04 mL/min/kg).

The toxicity predictions differentiated the series more clearly. All compounds showed low predicted cardiotoxicity liability, with minimal hERG-blocking potential (probability = 0.09–0.25). In contrast, compound **31** displayed a high predicted DILI risk (0.97), plausibly associated with the thiophene ring, a known structural

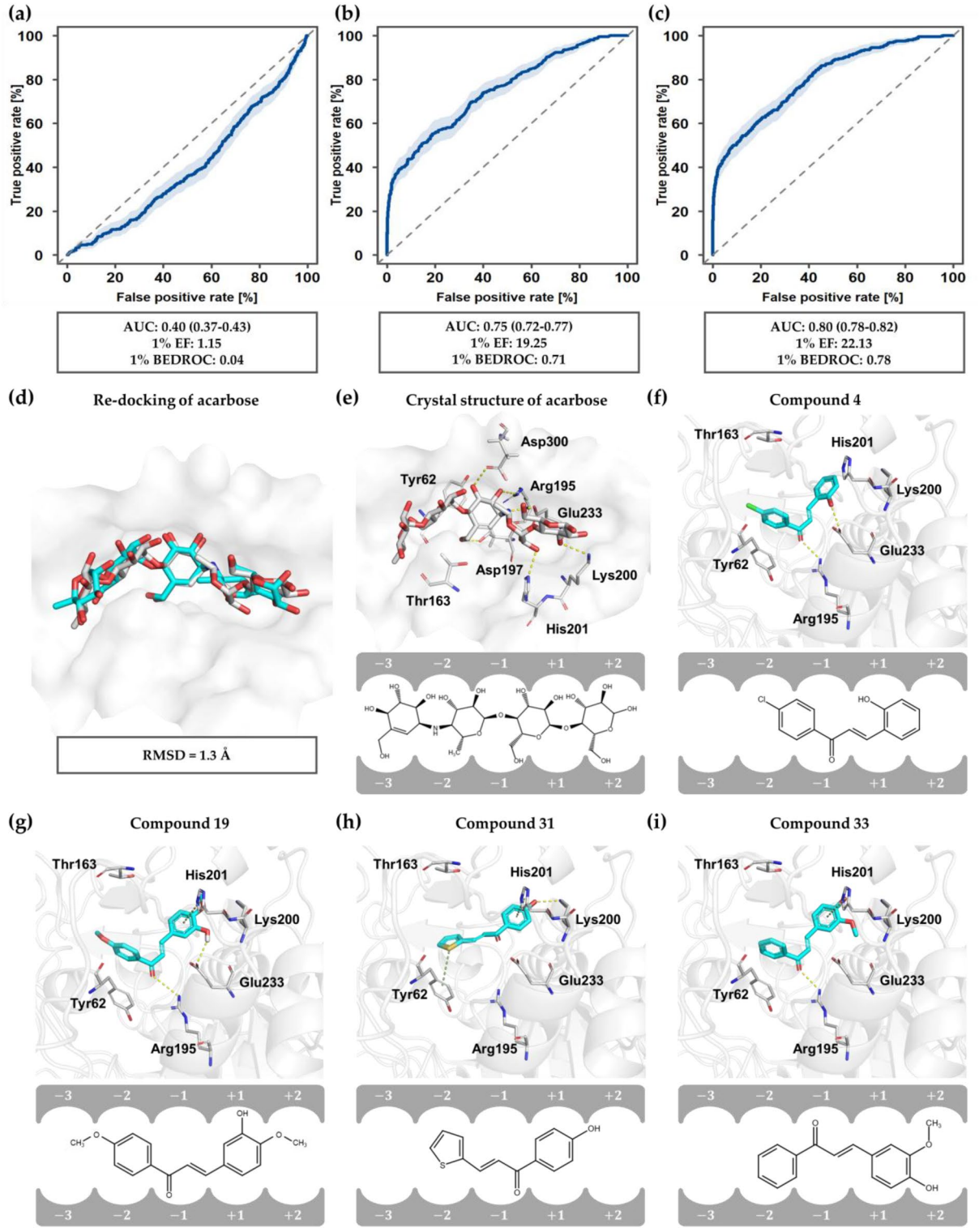

Fig. 3. Validation of the docking protocol and predicted binding modes of the most active chalcone derivatives in α-amylase. (**a**) ROC curve for standard docking using the Docking Score function. (**b**) ROC curve for Naive Bayes rescoring based on genetic algorithm-selected docking descriptors. (**c**) ROC curve for ensemble docking combined with Naive Bayes rescoring after incorporation of four representative protein conformations generated by CABS-flex. (**d**) Superposition of the crystallographic and re-docked poses of acarbose (RMSD = 1.3 Å). (**e**) Crystallographic binding mode of acarbose in the α-amylase active site. (**f–i**) Predicted binding modes of compounds **4**, **19**, **31**, and **33**, respectively. Hydrogen bonds are shown in yellow, π–π interactions in green, and the protein surface in gray.

Cpd	logS	logD	logP	Caco-2	PAMPA	HLM	CLplasma	hERG	DILI	Ames
4	-4.41	3.42	3.75	🟢 (-4.63)	🟢 (0.06)	🟡 (0.3)	🟡 (7.79)	🟢 (0.25)	🟡 (0.64)	🟢 (0.15)
19	-2.61	2.0	2.21	🔴 (-5.15)	🟢 (0.11)	🟡 (0.31)	🟡 (7.53)	🟢 (0.09)	🟡 (0.37)	🟡 (0.56)
31	-3.31	3.12	2.95	🟢 (-4.75)	🟢 (0.16)	🟡 (0.61)	🟢 (11.04)	🟢 (0.23)	🔴 (0.97)	🟡 (0.49)
33	-3.52	3.14	3.01	🟢 (-4.84)	🟢 (0.01)	🟡 (0.37)	🟢 (10.15)	🟢 (0.21)	🟡 (0.49)	🟡 (0.32)

Table 2. In silico ADMET profile for top compounds. Color coding indicates favorable (green), intermediate (yellow), and unfavorable (red) predicted profiles, with numerical values shown in parentheses. Reference criteria were: logS, − 4 to 0.5; logD, 1–3; logP, 0–3; Caco-2, > − 5.15 log cm/s; CLplasma, < 5 low, 5–15 moderate, and > 15 high; and, for all probability-based endpoints (PAMPA, HLM instability, hERG, DILI, and AMES), 0–0.3 favorable, 0.3–0.7 intermediate, and 0.7–1.0 unfavorable.

alert for bioactivation. Compounds **4**, **19**, and **33** showed moderate hepatotoxicity risk (0.37–0.64), which may be related to the intrinsic Michael acceptor character of the chalcone enone system. Predicted AMES mutagenicity was lowest for compound **4** (0.15), whereas **19**, **31**, and **33** showed intermediate probabilities (0.32–0.56), supporting the need for experimental genotoxicity assessment during prospective studies. In summary, these results confirm compound **4** as the most balanced ADMET hit for prospective hit-to-lead investigations.

Conclusions

In this work, a combined synthetic, biological, and computational workflow identified chalcone derivatives with α-amylase inhibitory activity and DPPH radical-scavenging properties. A library of 40 chalcone analogs was synthesized, characterized, and evaluated in vitro, leading to the identification of compound **4** as the most promising hit in the series. Structure-based analysis with a validated ensemble and Naive Bayes scoring suggested that compounds **4**, **19**, **31**, and **33** binds effectively within the α-amylase catalytic groove, with an interaction with Glu233 directly interfering with the enzyme's hydrolytic mechanism, explaining its increased inhibitory potency. In silico ADMET profiling further indicated acceptable developability features for the hit compounds, including suitable solubility, intestinal permeability, and low predicted cardiotoxicity, with compound **4** showing the most balanced overall profile. In summary, these findings identify this chalcone series as a promising starting point for hit-to-lead optimization toward multifunctional radical-scavenging and α-amylase-inhibitory activities.

Data availability

All data generated or analysed during this study are included in this published article and its supplementary information file.

Received: 19 January 2026; Accepted: 26 May 2026
Published online: 24 June 2026

References

1. DeFronzo, R. A. et al. Type 2 diabetes mellitus. *Nat. Rev. Dis. Primers* **1**, 1–22 (2015).
2. Udrea, A. M. et al. Advanced bioinformatics tools in the pharmacokinetic profiles of natural and synthetic compounds with anti-diabetic activity. *Biomolecules* **11**, 1692 (2021).
3. Kanwal Khan, K. M. et al. Indole-3-acetamides: As potential antihyperglycemic and antioxidant agents; synthesis, in vitro α-amylase inhibitory activity, structure–activity relationship, and in silico studies. *ACS Omega* **6**, 2264–2275 (2021).
4. Association, A. D. Diagnosis and classification of diabetes mellitus. *Diabetes Care* **37**(Supplement_1), S81–S90 (2014).
5. Proença, C., Ribeiro, D., Freitas, M. & Fernandes, E. Flavonoids as potential agents in the management of type 2 diabetes through the modulation of α-amylase and α-glucosidase activity: A review. *Crit. Rev. Food Sci. Nutr.* **62**, 3137–3207 (2022).
6. Zawudie, A. B., Daka, D. W., Teshome, D. & Ergiba, M. S. Economic burden of diabetic mellitus among patients on follow-up care in hospitals of Southwest Shewa Zone, central Ethiopia. *BMC Health Serv. Res.* **22**, 1398 (2022).
7. Addanki, H. R. et al. An in silico ADMET, molecular docking study and microwave-assisted synthesis of new phosphorylated derivatives of thiazolidinedione as potential anti-diabetic agents. *Synth. Commun.* **52**, 300–315 (2022).
8. Singh, R. et al. Parsing structural fragments of thiazolidin-4-one based α-amylase inhibitors: a combined approach employing in vitro colorimetric screening and GA-MLR based QSAR modelling supported by molecular docking, molecular dynamics simulation and ADMET studies. *Comput. Biol. Med.* **157**, 106776 (2023).
9. Imran, A. et al. Development, molecular docking, and in silico ADME evaluation of selective ALR2 inhibitors for the treatment of diabetic complications via suppression of the polyol pathway. *ACS Omega* **7**, 26425–26436 (2022).
10. Janeček, Š, Svensson, B. & MacGregor, E. A. A., α-Amylase: An enzyme specificity found in various families of glycoside hydrolases. *Cell. Mol. Life Sci.* **71**, 1149–1170 (2014).
11. Martinez-Gonzalez, A. I. et al. Polyphenolic compounds and digestive enzymes: In vitro non-covalent interactions. *Molecules* **22**, 669 (2017).
12. Sales, P. M. D., Souza, PMd., Simeoni, L. A., Batista, Pd. O. M. D. & Silveira, D. α-Amylase inhibitors: a review of raw material and isolated compounds from plant source. *J. Pharm. Pharm. Sci.* **15**, 141–183 (2012).
13. Kursun Aktar, B. S. et al. Discovery of novel pyrrolidine-based chalcones as dual inhibitors of α-amylase and α-glucosidase: synthesis, molecular docking, ADMET profiles, and pharmacological screening. *ACS Omega* **10**(9), 9368–9380 (2025).
14. Jadhav, N. C., Pahelkar, A. R., Desai, N. V. & Telvekar, V. N. Design, synthesis and molecular docking study of novel pyrrole-based α-amylase and α-glucosidase inhibitors. *Med. Chem. Res.* **26**, 2675–2691 (2017).

15. Rocha, S. et al. A study towards drug discovery for the management of type 2 diabetes mellitus through inhibition of the carbohydrate-hydrolyzing enzymes α-amylase and α-glucosidase by chalcone derivatives. *Food Funct.* **10**, 5510–5520 (2019).
16. Chen, N. & Karantza-Wadsworth, V. Role and regulation of autophagy in cancer. *Biochimica et Biophysica Acta (BBA)* **1793**, 1516–1523 (2009).
17. Gonzalez, C. D. et al. The emerging role of autophagy in the pathophysiology of diabetes mellitus. *Autophagy* **7**, 2–11 (2011).
18. Hara, T. et al. Suppression of basal autophagy in neural cells causes neurodegenerative disease in mice. *Nature* **441**, 885–889 (2006).
19. Krakauer, T. Inflammasome, mTORC1 activation, and metabolic derangement contribute to the susceptibility of diabetics to infections. *Med. Hypotheses* **85**, 997–1001 (2015).
20. Zhang, Y. et al. Prevention of hyperglycemia-induced myocardial apoptosis by gene silencing of Toll-like receptor-4. *J. Transl. Med.* **8**, 1–8 (2010).
21. Boyd, N. & McGuire, V. The possible role of lipid peroxidation in breast cancer risk. *Free Radic. Biol. Med.* **10**, 185–190 (1991).
22. Kushi, L. H. et al. Dietary antioxidant vitamins and death from coronary heart disease in postmenopausal women. *N. Engl. J. Med.* **334**, 1156–1162 (1996).
23. Omenn, G. S. et al. Effects of a combination of beta carotene and vitamin A on lung cancer and cardiovascular disease. *N. Engl. J. Med.* **334**, 1150–1155 (1996).
24. Riemersma, R. et al. Anti-oxidants and pro-oxidants in coronary heart disease. *Lancet* **337**, 677 (1991).
25. Stephens, N. G. et al. Randomised controlled trial of vitamin E in patients with coronary disease: Cambridge Heart Antioxidant Study (CHAOS). *Lancet* **347**, 781–786 (1996).
26. Street, D. A., Comstock, G. W., Salkeld, R. M., Schüep, W. & Klag, M. J. Serum antioxidants and myocardial infarction. Are low levels of carotenoids and alpha-tocopherol risk factors for myocardial infarction?. *Circulation* **90**, 1154–1161 (1994).
27. Di Rosa, M., Distefano, G., Gagliano, C., Rusciano, D. & Malaguarnera, L. Autophagy in diabetic retinopathy. *Curr. Neuropharmacol.* **14**, 810–825 (2016).
28. Kohnert, K.-D., Freyse, E.-J. & Salzsieder, E. Glycaemic variability and pancreatic ß-cell dysfunction. *Curr. Diabetes Rev.* **8**, 345–354 (2012).
29. Liang, W. et al. A novel damage mechanism: Contribution of the interaction between necroptosis and ROS to high glucose-induced injury and inflammation in H9c2 cardiac cells. *Int. J. Mol. Med.* **40**, 201–208 (2017).
30. Bansal, Y. & Silakari, O. Multifunctional compounds: smart molecules for multifactorial diseases. *Eur. J. Med. Chem.* **76**, 31–42 (2014).
31. Noureddin, S. A., El-Shishtawy, R. M. & Al-Footy, K. O. Curcumin analogues and their hybrid molecules as multifunctional drugs. *Eur. J. Med. Chem.* **182**, 111631 (2019).
32. Zhang, C., Lv, Y., Bai, R. & Xie, Y. Structural exploration of multifunctional monoamine oxidase B inhibitors as potential drug candidates against Alzheimer's disease. *Bioorg. Chem.* **114**, 105070 (2021).
33. Alam, M. S., Rahman, S. M. & Lee, D.-U. Synthesis, biological evaluation, quantitative-SAR and docking studies of novel chalcone derivatives as antibacterial and antioxidant agents. *Chem. Pap.* **69**, 1118–1129 (2015).
34. Karthikeyan, C. et al. Advances in chalcones with anticancer activities. *Recent Pat. Anti-Canc. Drug Discov.* **10**, 97–115 (2015).
35. Elkanzi, N. A. et al. Synthesis of chalcones derivatives and their biological activities: a review. *ACS Omega* **7**, 27769–27786 (2022).
36. Ali, A. et al. Dihydropyrazole derivatives act as potent α-amylase inhibitors and free radical scavengers: synthesis, bioactivity evaluation, structure–activity relationship, ADMET, and molecular docking studies. *ACS Omega* **8**, 20412–20422 (2023).
37. Saleem, F. et al. Synthesis of azachalcones, their α-amylase, α-glucosidase inhibitory activities, kinetics, and molecular docking studies. *Bioorg. Chem.* **106**, 104489 (2021).
38. Abd El-Sattar, N. E., Badawy, E. H. & Abdel-Mottaleb, M. Synthesis of some pyrimidine, pyrazole, and pyridine derivatives and their reactivity descriptors. *J. Chem.* https://doi.org/10.1155/2018/8795061 (2018).
39. Ovonramwen, O. B., Owolabi, B. J. & Oviawe, A. P. Recent advances in chalcones: Synthesis, transformation and pharmacological activities. *Asian J. Chem. Sci.* **6**, 1–16 (2019).
40. Ramawat, K. G. & Mérillon, J.-M. *Natural Products* (Springer-Verlag Berlin Heidelberg, 2013).
41. Xu, Y., Ahmad, N., Muhammad, Y. & Wang, L. Promising anti-inflammatory effects of chalcones via inhibition of cyclooxygenase, prostaglandin E 2, inducible NO synthase and nuclear factor κb activities. *Bioorg. Chem.* **87**, 335–365 (2019).
42. Ibrahim, T. S. et al. Novel chalcone/aryl carboximidamide hybrids as potent anti-inflammatory via inhibition of prostaglandin E2 and inducible NO synthase activities: design, synthesis, molecular docking studies and ADMET prediction. *J. Enzyme Inhib. Med. Chem.* **36**, 1067–1078 (2021).
43. Lakshminarayanan, B., Kannappan, N. & Subburaju, T. Synthesis and biological evaluation of novel chalcones with methanesulfonyl end as potent analgesic and anti-inflammatory agents. *Int. J. Pharmaceutical Res. Biosci.* **11**, 4974–4981 (2020).
44. Čižmáriková, M. et al. New chalcone derivative inhibits ABCB1 in multidrug resistant T-cell lymphoma and colon adenocarcinoma cells. *Anticancer Res.* **39**, 6499–6505 (2019).
45. Choudhary, A., Kumar, A. & Juyal, V. Design, synthesis and evaluation of chalcone derivatives as anti-inflammatory, antioxidant and antiulcer agents. *Lett. Drug Des. Discov.* **9**, 479–488 (2012).
46. Fu, Y. et al. New chalcone derivatives: synthesis, antiviral activity and mechanism of action. *RSC Adv.* **10**(41), 24483–24490 (2020).
47. Alsafi, M. A., Hughes, D. L. & Said, M. A. First COVID-19 molecular docking with a chalcone-based compound: synthesis, single-crystal structure and Hirshfeld surface analysis study. *Acta Crystallogr. C Struct. Chem.* **76**, 1043–1050 (2020).
48. Okolo, E. N. et al. New chalcone derivatives as potential antimicrobial and antioxidant agent. *Sci. Rep.* **11**, 21781 (2021).
49. Henry, E. J., Bird, S. J., Gowland, P., Collins, M. & Cassella, J. P. Ferrocenyl chalcone derivatives as possible antimicrobial agents. *J. Antibiot.* **73**, 299–308 (2020).
50. Aljohani, G., Al-Sheikh Ali, A., Alraqa, S. Y., Itri Amran, S. & Basar, N. Synthesis, molecular docking and biochemical analysis of aminoalkylated naphthalene-based chalcones as acetylcholinesterase inhibitors. *J. Taibah Univ. Sci.* **15**, 781–797 (2021).
51. Al Zahrani, N. A., El-Shishtawy, R. M., Elaasser, M. M. & Asiri, A. M. Synthesis of novel chalcone-based phenothiazine derivatives as antioxidant and anticancer agents. *Molecules* **25**, 4566 (2020).
52. Vanangamudi, G., Subramanian, M. & Thirunarayanan, G. Synthesis, spectral linearity, antimicrobial, antioxidant and insect antifeedant activities of some 2, 5-dimethyl-3-thienyl chalcones. *Arab. J. Chem.* **10**, S1254–S1266 (2017).
53. Cai, C.-Y. et al. Analogues of xanthones——Chalcones and bis-chalcones as α-glucosidase inhibitors and anti-diabetes candidates. *Eur. J. Med. Chem.* **130**, 51–59 (2017).
54. Fang, Q. et al. Attenuation of inflammatory response by a novel chalcone protects kidney and heart from hyperglycemia-induced injuries in type 1 diabetic mice. *Toxicol. Appl. Pharmacol.* **288**, 179–191 (2015).
55. Jain, A. & Jain, D. Synthesis, characterization and biological evaluation of some new heterocyclic derivatives of chalcone as antihyperglycemic agents. *Int. J. Pharm. Sci. Res.* **59**, 5700–5706 (2019).
56. Hameed, A. et al. Anti-HIV cytotoxicity enzyme inhibition and molecular docking studies of quinoline based chalcones as potential non-nucleoside reverse transcriptase inhibitors (NNRT). *Bioinorg. Chem.* **65**, 175–182 (2016).
57. Escrivani, D. O. et al. Chalcones identify cTXNPx as a potential antileishmanial drug target. *PLoS Negl. Trop. Dis.* **15**, e0009951 (2021).
58. Bhoj, P. et al. Immunomodulatory activity of sulfonamide chalcone compounds in mice infected with filarial parasite, *Brugia malayi*. *Indian J. Clin. Biochem.* **34**, 225–229 (2019).

59. Qin, H.-L., Zhang, Z.-W., Lekkala, R., Alsulami, H. & Rakesh, K. Chalcone hybrids as privileged scaffolds in antimalarial drug discovery: a key review. *Eur. J. Med. Chem.* **193**, 112215 (2020).
60. K Sahu, N., S Balbhadra, S., Choudhary, J. & V Kohli, D. Exploring pharmacological significance of chalcone scaffold: a review. *Curr. Med. Chem.* **19**, 209–225 (2012).
61. Aktar, B. S. K., Adem, Ş, Ekinci, E. & Oruç-Emre, E. E. Design, synthesis, tyrosinase inhibitors activities and molecular docking of novel methylated chalcones and pyrazoles having a pyrrolidine ring. *J. Mol. Struct.* **1340**, 142494 (2025).
62. Beltramino, R., Penenory, A. & Buceta, A. M. An open-label, randomized multicenter study comparing the efficacy and safety of Cyclo 3 Fort® versus hydroxyethyl rutoside in chronic venous lymphatic insufficiency. *Angiology* **51**, 535–544 (2000).
63. Santos, D. C. et al. Apoptosis oxidative damage-mediated and antiproliferative effect of selenylated imidazo[1,2-a]pyridines on hepatocellular carcinoma HepG2 cells and in vivo. *J. Biochem. Mol. Toxicol.* **35**, e22663 (2021).
64. Pedroso, G. J. et al. Selenylated indoles: synthesis, effects on lipid membrane properties and DNA cleavage. *New J. Chem.* **47**, 2719–2726 (2023).
65. Frizon, T. E. A. et al. Synthesis of novel selenocyanates and evaluation of their effect in cultured mouse neurons submitted to oxidative stress. *Oxid. Med. Cell. Longev.* **2020**, 5417024 (2020).
66. Botteselle, G. V. et al. catalytic antioxidant activity of bis-aniline-derived diselenides as GPx mimics. *Molecules* **26**, 4446 (2021).
67. Doerner, C. V. et al. Versatile electrochemical synthesis of selenylbenzo[b]furan derivatives through the cyclization of 2-alkynylphenols. *Front. Chem.* **10**, 880099 (2022).
68. Tornquist, B. L. et al. Ytterbium (III) triflate/Sodium Dodecyl Sulfate: a versatile recyclable and water-tolerant catalyst for the synthesis of Bis(indolyl)methanes (BIMs). *ChemistrySelect* **3**, 6358–6363 (2018).
69. Santos, D. C. et al. IP-Se-06, a selenylated imidazo[1,2-a]pyridine, modulates intracellular redox state and causes Akt/mTOR/HIF-1α and MAPK signaling inhibition, promoting antiproliferative effect and apoptosis in Glioblastoma cells. *Oxid. Med. Cell. Longev.* https://doi.org/10.1155/2022/3710449 (2022).
70. Lourenço, E. M. G. et al. Flavonoid derivatives as new potent inhibitors of cysteine proteases: an important step toward the design of new compounds for the treatment of leishmaniasis. *Microorganisms* **11**, 225 (2023).
71. Gomes, G. B. et al. Selenylated imidazo [1,2-a]pyridine induces apoptosis and oxidative stress in 2D and 3D models of colon cancer cells. *Pharmaceuticals* **16**, 814 (2023).
72. Veloso, I. C. et al. A selanylimidazopyridine (3-SePh-IP) reverses the prodepressant- and anxiogenic-like effects of a high-fat/high-fructose diet in mice. *J. Pharm. Pharmacol.* **73**, 673–681 (2021).
73. Shah, M. I. A., Khan, R., Arfan, M., Wadood, A. & Ghufran, M. Synthesis, in vitro urease inhibitory activity and molecular docking of 3, 5-disubstituted thiadiazine-2-thiones. *J. Heterocycl. Chem.* **56**, 3073–3080 (2019).
74. Tamanna, et al. Thiadiazine thione derivatives as anti-leishmanial agents: synthesis, biological evaluation, structure activity relationship, ADMET, molecular docking and molecular dynamics simulation studies. *J. Biomol. Struct. Dyn.* **42**, 7758–7772 (2024).
75. Haroon, M. et al. Alkyl 2-(2-(arylidene) alkylhydrazinyl) thiazole-4-carboxylates: synthesis, acetyl cholinesterase inhibition and docking studies. *J. Mole. Struct.* **1245**, 131063 (2021).
76. Fermiano, M. H. et al. Selenium-containing (hetero)aryl hybrids as potential antileishmanial drug candidates: in vitro screening against *L. amazonensis*. *Biomedicines* **12**, 213 (2024).
77. Burkner, G. T. et al. Selenylated Imidazo[1,2-*a*]pyridine induces cell senescence and oxidative stress in chronic myeloid leukemia cells. *Molecules* **28**, 893 (2023).
78. Lourenço, E. M. G. et al. Flavonoid derivatives as new potent inhibitors of cysteine proteases: an important step toward the design of new compounds for the treatment of leishmaniasis. *Microorganisms* **11**, 225 (2023).
79. Suma, T., Adnin, A. & Wahyuningsih, T. D. Efficient synthesis of chloro chalcones under ultrasound irradiation, their anticancer activities and molecular docking studies. *Rasayan J. Chem.* **12**, 502–510 (2019).
80. Palleros, D. R. Solvent-free synthesis of chalcones. *J. Chem. Educ.* **81**, 1345 (2004).
81. Afonso, C. A. et al. *Comprehensive Organic Chemistry Experiments for the Laboratory Classroom* (Royal Society of Chemistry, 2020).
82. Rashdan, S. A., Hassan, A. M., Mandeel, Q. A., Alasfoor, N. M. & Dawood, Z. H. Synthesis of substituted chalcones and investigation of their biological activities. *J. Chem.* **6**, 1–8 (2018).
83. Zheng, C. J., Jiang, S. M., Chen, Z. H., Ye, B. J. & Piao, H. R. Synthesis and anti-bacterial activity of some heterocyclic chalcone derivatives bearing thiofuran, furan, and quinoline moieties. *Arch. Pharm.* **344**, 689–695 (2011).
84. Rachmale, P. Synthesis and antimicrobial activity of some chalcone derivatives and their coppercomplexes. *Int. J. Pharm. Sci. Res.* **3**, 901 (2012).
85. Han Lee, I.-S., Jeoung, E. J. & Lee, C. K. Synthesis and NMR Studies of (E)-1-Aryl-3-(2-pyrrolyl)-2-propenones and (E)-3-Aryl-1-(2-pyrrolyl)-2-propenones. *Bull. Korean Chem. Soc.* **34**, 936–942 (2013).
86. Mojarrab, M., Soltani, R. & Aliabadi, A. Pyridine based chalcones: Synthesis and evaluation of antioxidant activity of 1-phenyl-3-(pyridin-2-yl) prop-2-en-1-one derivatives. *Jundishapur J. Nat. Pharm. Prod.* **8**, 125 (2013).
87. Bandgar, B. P., Gawande, S. S., Bodade, R. G., Totre, J. V. & Khobragade, C. N. Synthesis and biological evaluation of simple methoxylated chalcones as anticancer, anti-inflammatory and antioxidant agents. *Bioorg. Med. Chem.* **18**, 1364–1370 (2010).
88. Bradley, A. & Ashburn, O. Synthesis and antimicrobial evaluation of a series of chlorinated chalcone derivatives. *Int. J. Pharm. Sci. Res.* **13**, 112–119 (2018).
89. Liu, M., Wilairat, P. & Go, M.-L. Antimalarial alkoxylated and hydroxylated chalones: structure– activity relationship analysis. *J. Med. Chem.* **44**, 4443–4452 (2001).
90. Syam, S., Abdelwahab, S. I., Al-Mamary, M. A. & Mohan, S. Synthesis of chalcones with anticancer activities. *Molecules* **17**, 6179–6195 (2012).
91. Rashid, H. et al. Direct synthesis, characterization, in vitro and in silico studies of simple chalcones as potential antimicrobial and antileishmanial agents. *R. Soc. Open Sci.* **11**, 240410 (2024).
92. Hasan, A. H. Synthesis of chalcone derivatives and evaluation their biological activities. *J. Garmian Univ.* **1**, 582–593 (2016).
93. Singh, P., Anand, A. & Kumar, V. Recent developments in biological activities of chalcones: a mini review. *Eur. J. Med. Chem.* **85**, 758–777 (2014).
94. Custodio, J. M. et al. The influence of methoxy and ethoxy groups on supramolecular arrangement of two methoxy-chalcones. *J. Braz. Chem. Soc.* **28**, 2180–2191 (2017).
95. Chougale, U., Kharade, P. & Dhongade, S. Synthesis of some chalcone derivatives and screening of their antimicrobial activity. *Res. J. Life Sci. Bioinform. Pharm. Chem. Sci.* **5**, 344 (2019).
96. Mandge, S., Singh, H. P., Gupta, S. D. & Moorthy, N. Synthesis and characterization of some chalcone derivatives. *Trends Appl. Sci. Res.* **2**, 52–56 (2007).
97. Suwunwong, T., Chantrapromma, S. & Fun, H.-K. Influence of trimethoxy-substituted positions on fluorescence of heteroaryl chalcone derivatives. *Chem. Pap.* **65**, 890–897 (2011).
98. Mathew, B. et al. Synthesis, ADME studies, toxicity estimation, and exploration of molecular recognition of thiophene based chalcones towards monoamine oxidase-A and B. *Beni-Suef Univ. J. Basic Appl. Sci.* **5**(4), 396–401 (2016).
99. Chelladurai, G. R. M. & Chinnachamy, C. Alpha amylase and alpha glucosidase inhibitory effects of aqueous stem extract of *Salacia oblonga* and its GC-MS analysis. *Braz. J. Pharm. Sci.* **54**, e17151 (2018).

100. Jung, H. J. et al. Design, synthesis, and antioxidant and anti-tyrosinase activities of (*Z*)-5-Benzylidene-2-(naphthalen-1-ylamino) thiazol-4(5*H*)-one analogs: In vitro and in vivo insights. *Molecules* **30**, 289 (2025).
101. Brand-Williams, W., Cuvelier, M. E. & Berset, C. Use of a free radical method to evaluate antioxidant activity. *LWT* **28**, 25–30 (1995).
102. Nahoum, V. et al. Crystal structures of human pancreatic alpha-amylase in complex with carbohydrate and proteinaceous inhibitors. *Biochem. J.* **15**, 201–208 (2000).
103. Shelley, J. C. et al. Epik: A software program for pK a prediction and protonation state generation for drug-like molecules. *J. Comput. Aided Mol. Des.* **21**, 681–691 (2007).
104. Olsson, M. H. M., Søndergaard, C. R., Rostkowski, M. & Jensen, J. H. PROPKA3: Consistent treatment of internal and surface residues in empirical PKA predictions. *J. Chem. Theory Comput.* **7**, 525–537 (2011).
105. Banks, J. L. et al. Integrated modeling program, applied chemical theory (IMPACT). *J. Comput. Chem.* **26**, 1752–1780 (2005).
106. Wróblewski, K., Zalewski, M., Kuriata, A. & Kmiecik, S. CABS-flex 3.0: An online tool for simulating protein structural flexibility and peptide modeling. *Nucleic Acids Res.* **53**, W95–W101 (2025).
107. Alberca, L. N. et al. LIDEB's useful decoys (LUDe): a freely available decoy-generation tool. Benchmarking and scope. *Artif. Intell. Life Sci.* https://doi.org/10.1016/j.ailsci.2025.100129 (2025).
108. Xiong, G. et al. ADMETlab 2.0: An integrated online platform for accurate and comprehensive predictions of ADMET properties. *Nucleic Acids Res.* **49**, W5–W14 (2021).
109. Neves BJ, Mottin M, Moreira-Filho JT, de Paula Sousa BK, Mendonca SS, Andrade CH. Best practices for docking-based virtual screening. In Molecular docking for computer-aided drug design Fundamentals, Techniques, Resources and Applications. (pp. 75-98). Academic Press. (2021).

Acknowledgements

The authors thank the Conselho Nacional de Desenvolvimento Científico e Tecnológico (CNPq), and Coordenação de Aperfeiçoamento de Pessoal de Nível Superior (CAPES).

Author contributions

Conceptualization: M.I.A.S., J.R., and S.S.; Methodology: A.A., F.B.O.D., G.R.R., and Z.H.; Validation: A.A., F.B.O.D., G.R.R., and Z.H.,; Formal analysis: A.Z., G.S.S.F., T.E.A.F., F.A.O., A.C., M.N., B.J.N., and M.I.A.S.; Investigation: .A., F.B.O.D., G.R.R., G.S.S.F. and B.J.N.; Resources: M.I.A.S., S.S., and J.R.; Data curation: A.A., F.B.O.D., G.R.R., Z.H. and T.E.A.F.; Writing—Original draft: M.I.A.S., J.R., and S.S.; Writing—Review & Editing: B.J.N., M.I.A.S., J.R., and S.S.,; Visualization: M.I.A.S., J.R., and J.R.; Supervision: M.I.A.S., J.R., and S.S.; Project administration: M.I.A.S., J.R., and S.S.; Funding acquisition: J.R., and S.S.

All authors read and approved the final draft of the manuscript.

Funding

We gratefully acknowledge CNPq, CAPES (001), and HEC (Pakistan) for financial support. J.R., and S.S., would like to acknowledge CNPq (308875/2026–5, 316687/2023–5, 309975/2022–0, 401355/2025–0, 404172/2023–7, and 405655/2023–1) for the Scholarships. B.J.N. was supported by CNPq (311100/2023–6). M.I.A.S. would like to acknowledge NRPU Project No. 17234. S.S. and J.R. also acknowledge the following FAPEG public calls: Chamada Pública FAPEG/SES Nº 18/2025 (ARB2025191000003), Chamada Pública FAPEG Nº 05/2025 (PVE2025041000055), and Chamada Pública FAPEG Nº 21/2025 (PEE2025331000083 and PEE2025331000108).

Competing interests

The authors declare no competing interests.

Additional information

Supplementary Information The online version contains supplementary material available at https://doi.org/10.1038/s41598-026-55706-3.

Correspondence and requests for materials should be addressed to M.I.A.S., J.R. or S.S.